A Sensorless IIoT Architecture Employing an Extended Kalman Filter as a Real-Time Virtual Sensor for Optimizing Progressive Cavity Pump Artificial Lift Systems

Acknowledgements

I want to express gratitude to my project supervisor, Prof. Sanjay Bahadoorsingh, for his invaluable guidance, technical insights and unwavering support throughout the course of this research. His constructive feedback was crucial in shaping the project's direction and maintaining the academic rigor necessary for its successful completion.

I would also like to extend my sincere thanks to my manager, Mr. Anand Ramsingh, for his support, encouragement and confidence in my professional and academic growth. His assistance in facilitating access to operational resources and offering flexibility throughout this study was invaluable.

Abstract

Optimizing Progressive Cavity Pump (PCP) artificial lift systems is limited by the challenge of observing downhole fluid submergence. Physical downhole sensors for direct measurement are often susceptible to failure in harsh environments while surface flowmeters can be economically and technically infeasible in heavy-oil, multiphase applications. This research introduces the design, implementation and field validation of a sensorless Industrial Internet of Things (IIoT) novel architecture that employs an Extended Kalman Filter (EKF) as a real-time virtual sensor to address this operational challenge.

A reduced-order, nonlinear state-space model was derived to correlate surface-measured mechanical torque and electrical parameters with the hydrostatic fluid load. The EKF was integrated with supervisory logic recognizing that purely statistical observers are prone to model mismatches during hydrodynamic transients, multiphase slugging and zero-speed periods. This hybrid architecture incorporates a state correction rate limit, friction torque interlock and anomaly detection to address these periods.

This proposed architecture was implemented on a heavy-oil production asset (Well X). The EKF submergence estimates were evaluated against independent acoustic surveys and a Root Mean Square Error (RMSE) of 54.3 m (178.16 ft) was calculated. This reflected an

error margin of 3.82% across the 1,420.4 m (4,660 ft) wellbore, establishing a novel benchmark for sensorless estimation accuracy. The ability to continuously estimate fluid levels enables operators to optimize pressure drawdown.

This operational optimization unlocks substantial and scalable commercial value. When assessed over a one year operational cycle for a full-scale fleet of 24 wells, this architecture yields a net one year revenue of USD $7,647,675.59 (TT$ 51,851,237.84). An estimated 5% increase in production results in aggregate Year 1 operating revenue of USD $7,726,320.00 (TT$ 52,384,450.00). Additionally, the deterministic interlock effectively mitigates the risk of catastrophic dry-run stator failures, leading to a cost avoidance of USD $3,000,000.00 (TT$ 20,340,000.00) per well.

Moreover, transitioning to this self-hosted LoRaWAN architecture delivers a consolidated annual savings on operational expenses amounting to TT$ 669,580.80 (USD $98,758.00). This is achieved by eliminating telemetry subscription fees and changing manual acoustic diagnostics to a semi-annual schedule, ultimately saving 1,920 labor hours each year.

While the system successfully achieved its design objectives, it is bounded by specific constraints. The reliance on static parameter approximations may introduce estimation bias during significant

reservoir shifts or long-term component wear, necessitating periodic recalibration. Furthermore, the telemetry update rate is restricted to five minutes and live closed loop speed modulation was limited to open loop validation to avoid inducing transient mechanical stress on the active rod string. Despite these challenges, the project successfully integrates nonlinear stochastic estimation with practical industrial automation thereby providing a resilient, lucrative solution for the intelligent control of PCPs.

Table of Contents

Acknowledgements....3

Abstract....4

1 Introduction....11

1.1 Aim....13

1.2 Objectives....13

1.3 Justification....14

1.4 Project Scope....15

1.4.1 Out of Scope....16

2 Literature Review....17

2.1 Fundamentals of Progressive Cavity Pumps....17

2.2 Operational Challenges of Progressive Cavity Pumps....18

2.3 Existing PCP Control Strategies....19

2.4 PCP Induction Motor Speed Control....28

2.5 PCP System Modeling....29

2.6 Kalman Filter Estimation....32

3 Methodology....36

3.1 Existing System Overview....36

3.2 IIoT System Architecture....39

3.3 PCP System Modeling....43

3.3.1 Derivation of the Reduced-order Hydrostatic Model....43

3.4 Extended Kalman Filter (EKF) Formulation....46

3.4.1 EKF Definitions....46

3.4.2 EKF Prediction....47

3.4.3 EKF Correction.....47
3.4.4 EKF Model Parameters.....49
3.5 System Implementation and Supervisory Control.....50
3.5.1 EKF Constraint Mechanisms.....50
3.5.2 Supervisory Speed Control Strategy.....51
3.5.3 Operator Interface Design.....51
3.6 Testing and Evaluation.....52
3.6.1 Virtual Sensor Validation.....53
3.6.2 Closed loop Speed Control (Bench-test).....55
3.6.3 Open loop Validation of Speed Control.....55
3.6.4 Closed Loop Speed Control Live Commissioning (Future).....56
3.6.5 Offline Computational Analysis (MATLAB).....57
4 Results and Discussion.....59
4.1 Evaluation Scenarios and Experimental Setup.....59
4.2 Well Profile and Baseline Initialization.....59
4.3 Steady-State Estimation.....60
4.4 Simulated Pump-Off Condition.....67
4.5 Transient Response: Pump Shutdown and Restart.....70
4.6 Open loop Validation of Speed Control.....75
4.7 Engineering and Financial Assessment.....78
4.7.1 Advantages over Prior Control Research.....78
4.7.2 Economics and Risk Mitigation.....79
4.7.3 Investment Feasibility.....82
4.8 Limitations and Future Work.....87
4.8.1 Limitations.....87

4.8.2 Recommendations for Future Work.....88
5 Conclusion.....90
6 References.....92
Appendix A.....97

List of Abbreviations

AI	Analog Input
CAPEX	Capital Expenditure
CHP	Casing Head Pressure
DI	Digital Input
DTC	Direct Torque Control
EKF	Extended Kalman Filter
FOC	Field-Oriented Control
HMI	Human-Machine Interface
ICM	Inflow Control Method
IIoT	Industrial Internet of Things
KF	Kalman Filter
LoRaWA	
N	Long Range Wide Area Network
LQR	Linear Quadratic Regulator
MAE	Mean Absolute Error
MAPE	Mean Absolute Percentage Error
	Message Queuing Telemetry
MQTT	Transport
OPEX	Operational Expenditure
PCP	Progressive Cavity Pump
PIP	Pump Intake Pressure
RMSE	Root Mean Square Error
RPM	Revolutions Per Minute
	Supervisory Control and Data
SCADA	Acquisition
THP	Tubing Head Pressure
VFD	Variable Frequency Drive
VSD	Variable Speed Drive

List of Figures

Figure 1: PCP Configuration.....11

Figure 2: Block Diagram for Direct torque control (DTC).....27

Figure 3: Surface and Subsurface components of a PCP system.....35

Figure 4: Block Diagram of Existing System.....37

Figure 5: Existing System Functional Diagram.....38

Figure 6: Block Diagram of Proposed System.....40

Figure 7: System Flow Diagram.....41

Figure 8: Plot of steady state parameters between 29 April 2026 and 4 May 2026.....61

Figure 9: Screen shot of Node-Red Live Dashboard illustrating Normal operations.....62

Figure 10: Plot showing the comparison between Manual fluid shot vs EKF estimate Submergence levels.....64

Figure 11: Plot of pump-off parameters between 11 February 2024 and 13 February 2024.....67

Figure 12: Dashboard screenshot illustrating a pump-off condition.....69

Figure 13: Plot of pump-off parameters between 30 March 2026 and 4 April 2026.....71

Figure 14: Dashboard screenshot illustrating PCP Off status.....74

Figure 15: Dashboard screenshot illustrating an Anomaly condition.....75

Figure 16: AVEVA HMI Screen for Well X.....76

Figure 17: VolleyBoast VoBo HL-1 Configuration Downlink Payload screenshot.....78

Figure 18: Node-RED Speed control nodes and Debug panel.....78

List of Tables

Table 1: Summary of previous PCP optimization and control research……22

Table 2: Summary of Testing and Evaluation.....57

Table 3: Comparison between Acoustic shot and EKF estimate submergence levels.....63

Table 4: CAPEX Per Well Breakdown.....81

Table 5: 5 Year Lifecycle Economic and Operational Value Assessment…..84

1 Introduction

The natural extraction of oil relies on the energy stored within the reservoir which is manifested as pressure in rocks and compressed fluids. As production advances and reservoirs deplete, there is a decline in the wells' production capacity. This decrease is attributed to the reduced ability by the reservoir to deliver fluid to the well as well as potential increases in pressure losses within the production column. When production demands cannot be met despite the availability of substantial reserves, artificial lift and secondary recovery techniques are employed to enhance output and elevate production levels. Various recovery methods for wells include gas lift, rod pumps, progressive cavity pumps (PCPs) and hydraulic pumping systems. The selection of an artificial lifting system is influenced by the well and reservoir characteristics, financial considerations and the well's location (Fotsa et al. 2024).

The rod pump uses a motor to drive a rod vertically thereby operating the pump. An electrical submersible pump (ESP) uses a downhole motor to power a centrifugal pump. Jet pumping boosts fluid flow by sending hydraulic liquid from the surface into the well. Gas lifting injects gas into a fluid column to increase its velocity and decrease density (Ceballos and Vivas 2019).

The PCP features a motor at the surface that powers a rod to operate a subsurface pump. The pump contains one helical rotor and a dual helical stator enclosed in elastomer. The rotation of the rotor creates sealed cavities that move fluids upward. A typical configuration of this system is depicted in Figure 1 .1 (Ceballos and Vivas 2019).

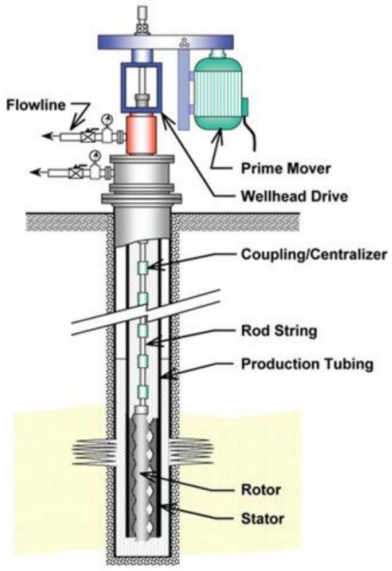

Figure 1.1: PCP Configuration

The PCP is a coupled electro-mechanical system. At the surface, the PCP drive system usually includes a thrust bearing to support the rod string, a stuffing box that seals around the polished rod to withstand pressure in the tubing and a powertrain comprising various combinations of gears, sheaves and belts. Additionally, there is a prime mover power source, commonly an electric motor or an internal combustion engine. Finally, the system features a braking mechanism for managing energy release when the drive is shut down (Wagg 2002).

The PCP's low output speed and progressive cavity transfer are beneficial to offshore separator installations due to its ability to manage the mixing of crude and water when compared to centrifugal pumps. (Lehman 2004). The main goal for PCP operators is to maximize fluid production without starving the pump, also known as "pump-off". Pump starvation could lead to stator damage and the requirement for an expensive workover intervention. (Woolsey 2012).

With the modernization of the petroleum industry, the integration of Variable Frequency Drives (VFDs) has enabled constant-speed operation for the improvement of mechanical efficiency. However, this change obscures downhole visibility and measured torque becomes the primary indicator of downhole hydraulic conditions (Takács 2010). Torque reflects a nonlinear combination of differential pressure and mechanical friction thus resulting in difficulties to distinguish between a transient gas slug and a legitimate fluid depletion event (Lea et al. 1999).

Virtual sensing techniques present a reliable alternative to overcome the limitations of using only surface measurements without resorting to costly downhole gauges. By leveraging the framework of the Kalman Filter, unmeasured downhole states can be estimated from surface data. In particular, the Extended Kalman Filter (EKF) which effectively manages the nonlinear relationship between wellbore hydrostatics and the measured surface torque (Welch and Bishop 2006).

1.1 Aim

The aim of this research is to develop and validate a sensorless framework for monitoring, protecting and improving the operation of PCP systems using open-source Industrial Internet of Things (IIoT) technologies and an Extended Kalman Filter for estimating downhole fluid submergence. Additionally, the methodology is assessed using field data from an active production PCP asset (Well X) to assess both estimation accuracy and practical applicability.

1.2 Objectives

This research proposes and validates a comprehensive strategy for optimizing production from speed-controlled PCP wells utilizing open-source Industrial IoT (IIoT) tools. This is achieved through the following objectives:

1. Perform a literature review on Progressive Cavity Pump (PCP) operation, dynamics and control.
2. Identify and model the mechanical, electrical and fluid dynamic characteristics of PCP systems.
3. Investigate, develop and implement a real-time virtual sensor by applying an Extended Kalman Filter (EKF) to the nonlinear hydrostatic model allowing for continuous downhole fluid submergence estimation.

4. Using the developed model, design and implement a closed loop control algorithm (operator-authorized) for PCP operation using open-source industrial automation tools and perform validation and verification of the developed system.

5. Compare the performance of the proposed control approach with existing field-tested or industry-standard PCP control strategies

6. Perform a technical and economic case study of this designed, developed and implemented solution for PCP well operation.

1.3 Justification

PCPs are currently employed as an artificial-lift method at several "Company X" well locations. At each site, the pumps are driven by induction motors controlled by ABB ACS800 VFDs. These drives utilize direct torque control (DTC) to regulate both motor speed and torque, thereby governing PCP operation.

Current PCP installations utilizing these speed-controlled VFDs are not fully optimized. They also lack automated systems for alarm and shutdown during pump-off conditions. The monitoring of these systems predominantly depends on proprietary tools which result in significant acquisition and maintenance costs.

1.4 Project Scope

The scope of this project includes the design, implementation and field validation of an EKF based virtual submergence sensor and supervisory control architecture via the technical boundaries:

- **Mathematical Modeling:** Developing a reduced-order, nonlinear state-space model that correlates surface-measured operational variables (motor torque, rotational speed, tubing pressure and casing pressure) to the unobservable downhole hydrostatic fluid load.
- **Virtual Sensor Development:** Designing and tuning a one-dimensional EKF stochastic observer to estimate fluid submergence in real-time. This phase also includes the establishment of pump state interlocks, state correction rate limiting and friction torque interlocks to ensure mathematical stability during non-linear transitions, pump-off conditions and zero-speed states.
- **IIoT Architecture and Integration:** Deployment of the hybrid control algorithm on an open-source, self-hosted programming tool (Node-RED), including the establishment of bi-directional telemetry routing utilizing MQTT, a ChirpStack network server and LoRaWAN protocols to interface with a commercial-off-the-shelf edge endpoint (VoBo HL).

- **Field Validation**: The assessment of the virtual sensor's performance using continuous live SCADA telemetry from an active, heavy-oil PCP asset (Well X). The estimator's steady-state submergence estimates are compared to independent acoustic fluid-level measurements. Additionally, the scope includes evaluating dynamic observer re-convergence during transient disruptions (scheduled shutdowns and restarts) and validating the deterministic pump-off interlock via identical EKF simulator.
- **Financial and Economic Assessment:** Performing a comprehensive one year operational revenue assessment that compares this proposed IIoT architecture against the existing proprietary third-party solution. This phase involves modeling Greenfield and Brownfield deployment scenarios, calculating capital expenditure (CAPEX) avoidance, mapping operational expenditure (OPEX) reductions, determining production enhancement revenue and developing an N+m hardware sparing strategy.

1.4.1 Out of Scope

The following elements are explicitly excluded from the research scope:

- **High-Fidelity Multiphase Modeling:** The research excludes the development of complex thermodynamic computational fluid dynamic (CFD) models. This system relies on a simplified,

lumped-parameter hydrodynamic approximation to ensure computational efficiency suitable for continuous IIoT execution.

- **Closed loop Actuation:** Autonomous closed loop speed modulation on the live asset is strictly excluded due to the availability the company's IT resources, stringent operational safety constraints and the severe mechanical risks associated with inducing transient stress on a producing rod string. Speed modulating validation is confined to open loop testing at this time where digital generation, protocol translation and network routing of Base64-encoded Modbus speed-control commands are analysed and confirmed.

2 Literature Review

2.1 Fundamentals of Progressive Cavity Pumps

The progressive cavity pump (PCP) originated in the 1920s by René Moineau who developed the helical pumping mechanism as part of his doctoral research on novel fluid displacement methods. This led to the establishment of PCM Pompes in 1932 which was the first commercial manufacturer of PCP systems (Lehman 2004).

In the 1980s, the oil and gas industry commenced adopting PCPs which were used to address the production challenges in heavy-oil reservoirs characterized by high viscosity and significant sand

production. Early PCP implementations encountered surface-drive limitations due to the torsional loading of sucker rods. Subsequently, the development of specialized driveheads improved field deployment reliability. PCPs were first widely installed in Canadian heavy-oil fields where conventional artificial-lift methods proved inadequate under abrasive and viscous conditions (Lehman 2004).

A typical PCP comprises a single helical rotor eccentrically rotating within a double-threaded elastomeric stator. The stator length is approximately twice the length of the rotor pitch. Sealed cavities are created via this geometric mismatch that progresses axially as the rotor rotates resulting in a continuous, non-pulsating flow (Saveth 1989; Nesbitt 2006). The downhole pump is driven by a surface prime mover through a rotating rod string where the produced fluids from the wellbore is lifted through the production tubing to the surface (Ceballos and Vivas 2019).

The pressure capability of a PCP is governed by the number of seal lines (stages) which is engineered to contribute a fixed pressure increment. Typical stage lengths range from 1.1 to 1.5 times the stator pitch length to facilitate adequate sealing and reasonable stator life (Saveth 1989). The increase in the number of stages or extension of the rotor-stator length enhances the achievable differential pressure thus enabling deeper installations and higher lift requirements. PCP systems

can achieve pressure differentials up to 40 bar and flow rates exceeding 300 m^3/h while handling viscous and abrasive fluids (Nesbitt 2006).

Slip losses in PCP operation are primarily a function of differential pressure and fluid properties. Slip is typically reduced by higher fluid viscosity but cavitation risk may be increased if suction conditions are inadequate. The elastomer compression fit is designed to remain constant over normal operating ranges with variations that may arise from wear or elastomer swelling (Saveth 1989). PCP stators are manufactured from natural rubber, nitrile, neoprene and Viton elastomers and are selected based on chemical compatibility, solids content and operating temperature (Nesbitt 2006).

PCPs handle oils ranging from approximately 8 °API to 45 °API and depths exceeding 2,000 m in regions such as Canada, Venezuela and Colombia (Lehman 2004; Ceballos and Vivas 2019). PCPs low-shear, positive-displacement mechanism minimizes emulsification thus improving downstream separation efficiency compared to centrifugal pumping systems (Lehman 2004).

2.2 Operational Challenges of Progressive Cavity Pumps

PCP systems are highly sensitive to pump-off conditions which occur when inflow to the pump is insufficient to maintain cavity fillage. During this condition, there is a loss of lubrication which leads to frictional heating, elastomer degradation and rapid stator failure. Pump-

off conditions often leads to the requirement of costly workover interventions (Woolsey 2012).

The maintenance of adequate fluid submergence above the pump intake is therefore critical. Historically, operators relied on manual fluid-level measurements to set pump speeds. However, these measurements provide instantaneous snapshots only and are prone to noise, gas interference and wellbore irregularities which has the potential to impact their usefulness for continuous control (Woolsey 2012). The operational risks of boosting sand and water production can be compounded by excessive drawdown when inflow is increased. (Ceballos and Vivas 2019).

The installation of downhole pressure and temperature sensors enable measurement of the pump intake pressure (PIP) and fluid level but incur high installation and maintenance costs. When these sensors fail, a workover of the entire well completion is typically required. This can also result in increased downtime and the possibility of stator damage (Romero et al. 2013; Klein et al. 1999). As a result, most PCP installations rely on surface-based measurements despite inherent limitations (Klein et al. 1999).

Torque inference using motor current has been widely employed as a non-intrusive indicator of pump load. However, PCP torque is influenced by multiple variables, including sand content, elastomer

swelling, fluid viscosity and multiphase flow, that make torque-only interpretation unreliable for detecting pump-off or inflow changes (Klein et al. 1999).

2.3 Existing PCP Control Strategies

Initial attempts to automate PCP operation focused primarily on preventing pump-off and extending equipment service life. One of the earliest optimization efforts was the Progressive Cavity Pump Optimization System (PCPOS) developed by (Klein et al. 1999). Field deployment of PCPOS demonstrated a 10 % increase in production and an extension of average pump run-life from 10 months to 18 months. This system established a direct physical correlation between the axial load measured at the surface drive and the hydraulic load of the downhole pump. The pump speed was regulated through a variable frequency drive (VFD) using an expert-system framework that incorporated fuzzy logic, neural networks, genetic algorithms and rule-based decision logic.

Further research highlighted flow-based control strategies. (Woolsey 2012) developed a patented controller that incrementally adjusted PCP speed while continuously monitoring produced fluid volume which increased outputs in several field implementations from 12 m^3/d to 145 m^3/d. They also reported that workovers eradicated for extended periods and pump efficiency was enhanced up to 74%. The approach assumed a linear relationship between pump speed and production when the cavities were filled. Additionally, secondary control algorithms were

implemented to enforce limits on torque, flow rate and pump efficiency which exhibited significant improvements in production. This method proved to be effective however, it relied on accurate surface flow measurement via wedge flowmeters and downhole submergence estimation was not provided.

(Romero et al. 2013) proposed a speed-based optimization methodology that varied pump RPM in predefined increments to infer well inflow capacity. They assumed that increasing the pump speed would result in a proportional increase in production for PCP wells. The setup incorporated a downhole sensor, wedge flowmeter, variable speed drive (VSD), pressure sensor, RPM sensor and SCADA interface for monitoring. (Romero et al. 2013) (Romero et al. 2013). Their approach enhanced the early detection of abnormal operating conditions but was dependent on downhole instrumentation.

(Eggers et al. 2013) developed an artificial neural network (ANN) framework to estimate daily production rates and identify underperforming PCP wells which reduced the time required to identify underperforming wells by approximately 20 %. They utilized both surface and downhole sensor inputs in a pilot study involving 50 wells. This method was effective for monitoring and diagnostics but did not report on the incorporation of physical constraints or pump-off control.

(Mehegan and Woolsey 2016) introduced the Liquid Inflow Control Method (ICM) which explicitly considers cavity fillage and pump slippage. They demonstrated an approach in which pump speed is gradually increased while monitoring flow to identify inflow conditions thereby facilitating the estimation of slippage and cavity fillage. They reported that their field implementation nearly doubled average daily water production, increased gas rates by approximately 60 % and reduced field staffing requirements by almost 70 %.

(Iguaran et al. 2021) applied a similar methodology as (Mehegan and Woolsey 2016) and reported production increases of up to 60 % within three months. Despite their success, ICM-based approaches require repeated inflow testing and rely on empirical interpretation of flow responses.

(Ceballos and Vivas 2019) integrated fuzzy logic, Linear Quadratic Regulation (LQR) and Kalman filter-based estimation techniques for production control in PCP systems. They utilized, surface measured torque, RPM and flow measurements in conjunction with downhole intake pressure sensors to estimate the fluid level above the pump and optimize pressure drawdown. A comparative analysis demonstrated that continuous LQR delivered superior production optimization while staying within torque limits. However, the fuzzy logic controllers showed sensitivity to noise and steady-state deviations. In examining their

methodology, physics-based estimation concepts were incorporated but relied on flow measurements via a wedge flowmeter.

Collectively, existing PCP control strategies illustrate that production optimization and pump-off mitigation can be achieved through heuristic, flow-based and data-driven methods. However, many of these approaches rely on empirical correlations, intermittent testing or expensive downhole instrumentation leaving a critical gap for a physics-based, continuous estimator capable of inferring downhole submergence solely from surface measurements. Table 2 .1 summarizes the major PCP optimization methodologies, hardware requirements, controller architectures and reported results from previous studies

Table 2.1: Summary of previous PCP optimization and control research

Author	Optimization Method	Equipment	Controller Details	Results
Klein et al. 1999	• Adjustment of the rotor's RPM based on the desired operational parameters input into the PCPOS. • Utilize the load supported by the axial bearing in the surface drive, along with various surface readings, to evaluate the dynamics of the PCP system in real-time.	• Surface drive containing an axial load measuring device and axial load bearing • Expert System software • VFD • PCP	• A C++ application that incorporates artificial intelligence techniques such as fuzzy logic, neural networks, genetic algorithms and expert systems. • A pattern recognition analysis is conducted on dynagraph, current and pressure charts, enabling diagnostic functions through an artificial self-organizing map neural network. • Target production rate is optimized using a genetic algorithm that identifies the most favorable operating conditions for the well, with control	• Demonstration of direct physical correlation between the axial load and the hydraulic load of the downhole pump • 10% increase in production and extended the average life of the PCP system from 10 months to 18 months. • A statistical error of +5.17% and -19.6% was achieved when compared to downhole sensors and sonic fluid level measurements respectively.

Author	Optimization Method	Equipment	Controller Details	Results
			actions derived from a comprehensive set of Fuzzy Logic rules.	
Woolsey 2012	• The patented control algorithm adjusts the pump speed in incremental steps while measuring the volume of fluid produced. • A linear correlation is established between fluid production and pump speed, provided that the pump cavities are completely filled with fluid from the pump intake.	• Wedge flowmeter • PCP controller • VFD • SCADA web system with real-time data	• The patented control algorithm. • Secondary control algorithms: 1. A polished-rod torque value to safeguard the rod string and pumping equipment. 2. A present flowrate value measured by the wedge flowmeter or another reliable flow measurement device. 3. A minimum pump efficiency limit ensuring that the pump operates above a certain efficiency threshold.	• Four field study implementation results 1. Oil production increase from 12 to 145m3/d and gas production from 19 to23 E3M3/D in 120 days. 2. Increase in well production from 2711m^3 and operational cost of USD 198,000 in a 6 month period to 19779m^3 with no workovers for the next 6 month period. 3. Limiting the maximum speed across four stages reduced sand to a manageable level, resulting in a revenue increase from USD 0/D to USD 7798/D and oil gain of 19.4m3/D. 4. Reduction in pump

Author	Optimization Method	Equipment	Controller Details	Results
				replacement from every 3 to 4 months along with 74% improvement in pump efficiency, oil gain of 1.84m^3/D and increase in oil revenue of USD 925/D.
Eggers el al. 2013	• Optimize well production rates through timely identification of underperformance occurrences.	• Down-hole and surface sensors	• ANNs using operational parameters measured in real time for estimating daily production rates of wells producing with PCPs.	• 20% reduction in the time required to identify underperforming wells, enabling easier detection of both underperforming and potentially problematic wells, along with insights into the likely causes of their issues.
Romero et al. 2013	• Modification of the RPM of the pump rod in predefined increments and measuring the production at these new speeds. • The premise was that an increase in the pump speed percentage for a well	• Downhole sensor • VSD • Wedge flowmeter • RPM sensor (Hall effect type sensor) • Pressure	• This research did not develop a controller/ control algorithm but configured a controller with a series of data such as the characteristics of the pump, the motor and the head of the	• 7% average increase in gross production within the period February - December 2012, maximum increase 20%. • Net production did not have significant changes, average increase of 0.27% and maximum increase of 20% coinciding with the

Author	Optimization Method	Equipment	Controller Details	Results
	utilizing a PCP should yield a corresponding percentage increase in the production rate.	sensor in the production line • SCADA interface collecting historical information	PCP, the type of VSD, analogical ranges of the intake sensors (flowmeters, pressure sensors, etc.) and outlet of the VSD control.	maximum gross production.
Mehegan and Woolsey 2016	• Liquid Inflow Control Method same as Iguaran et al.2021. • The pump speed is gradually increased while monitoring flow rates and cavity fillage until inflow is detected. • By comparing surface liquid production rates at two different speeds against the manufacturer’s theoretical pump displacement, an accurate value for pump slippage can be determined,	• Wedge flowmeter • RPM data - magnetic-style RPM sensor on the drive head booth and a magnet on the polish rod • Pump off controller with cellular connection	• Slowly ramps up the speed, monitoring flow and cavity fillage until inflow is detected. • When inflow is detected, the pump speed is reduced to match well inflow.	• Maintained optimal fluid level • Average daily water volume nearly doubled while gas rates increased approximately 60%. • Reduction in field staff by almost 70%. • Maximize production, increase the mean time between failures and better understand wells' capabilities.

Author	Optimization Method	Equipment	Controller Details	Results
	facilitating modeling of the pumping system.			
Iguaran et al. 2021	• Liquid Inflow Control Method - automatically tests the well to determine pump slippage and cavity fillage. • With this current pump information understood, it then adjusts the pump speed to determine the maximum well capacity or liquid well inflow. • Once well inflow is understood pump speed is adjusted to produce an outflow that matches the well inflow, or a fraction of the well inflow.	• Wedge flowmeter • Variable frequency drive • Optimization control panel	• The patented control algorithm varies the speed of the pump in steps while monitoring pump flow rate	• 60% production increase in 3 months.
Ceballos and Vivas 2019	• Continuously adjusts the RPM using fuzzy logic and measurement of the	• Rotation sensor • Torque sensor	• Fuzzy Logic with an output that controls the RPM.	• The fuzzy logic (FL) controller stabilized with a notable deviation from the reference

Author	Optimization Method	Equipment	Controller Details	Results
	downhole pump intake pressure. • A Kalman filter estimated the fluid level above the pump. • Maximized oil production through a Linear Quadratic Regulator (LQR) that managed pressure drawdown from the formation into the borehole.	• Wedge flowmeter		values. • The FL controller did not experience overshoot in torque but it exhibited overshoot in the fluid level. • The FL controller proved sensitive to noise, presenting significant torque overshoot and stabilizing at the peak torque value. • The continuous LQR demonstrated optimized production within torque levels • The discrete LQR had the longest stabilization time but achieved comparable steady-state flow rates.

2.4PCP Induction Motor Speed Control

Three-phase induction motors are widely used in PCP applications due to their robustness and compatibility with VSDs. Scalar (v/f) control regulates motor speed by maintaining a constant voltage-to-frequency ratio but lacks precision under variable load conditions (Ahmad and Le 2023).

Field-Oriented Control (FOC) improves dynamic performance by decoupling the torque and flux components of the stator current. However, FOC requires precise machine parameters and additional sensors. This results in increased system complexity and costs (Ahmad and Le 2023).

Direct Torque Control (DTC) directly estimates torque and flux from the measured stator voltages and currents. The ABB ACS800 VFD utilized in this research employs DTC thus its relevance to this research. DTC utilizes an adaptive motor model together with hysteresis controllers to optimize inverter switching states every 25 µs, DTC eliminates the requirement for PWM modulators (Tiitinen and Surandra 1996).

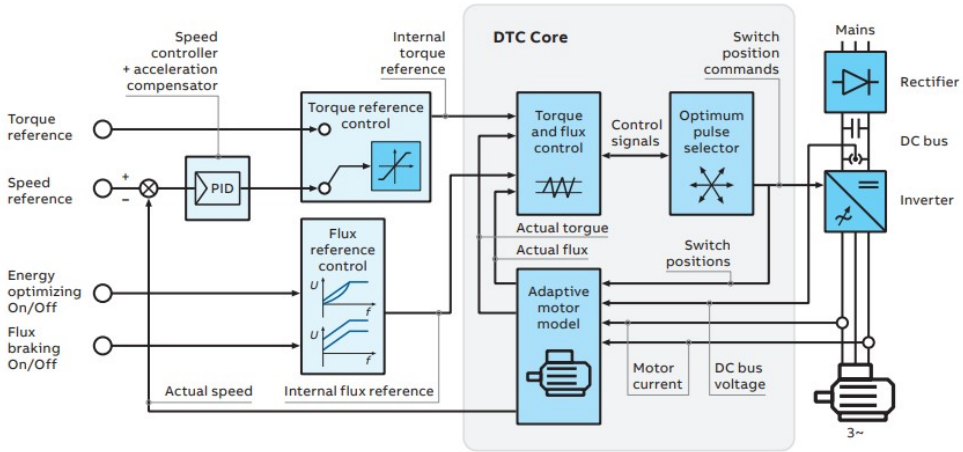

Figure 2.2: Block Diagram for Direct torque control (DTC)

The stator flux is estimated using feedback from the motor's voltage and current, while considering factors such as stator resistance, inverter non-idealities and thermal compensation. Torque is determined by the cross product of the stator flux and current vectors. Since rotor flux dynamics evolve more slowly than those of the stator flux, this allows for rapid torque control without the necessity of shaft-mounted sensors (Tiitinen and Surandra 1996).

2.5 PCP System Modeling

Full-order thermodynamic and multiphase flow models for PCPs are generally expressed as coupled nonlinear partial differential equations. These equations require fine spatial discretization, small integration time steps and iterative numerical solvers leading to significant computational complexity. This complexity arises from the models’ high dimensionality and nonlinearity. This ultimately limits their applicability in real-time IIoT-based monitoring and control systems (Kani and Elsheikh 2019).

Full physical fidelity is not essential for reconstructing an unmeasured state provided that the dominant input–output relationship is maintained. Reduced-order modeling techniques have been successfully integrated with Extended Kalman Filter (EKF) frameworks to enable real-time data assimilation and state estimation. This approach has demonstrated that

accurate state reconstruction can be achieved within a lower-dimensional representation of the system (Gonzalez et al. 2017).

Production engineering considers a well as an integrated production system that encompasses the reservoir, completion and production tubing and surface facilities. Within this framework, the pressure at any given point (or node) along the flow path is influenced by the combined effects of hydrostatic head and frictional losses occurring between the nodes. (Lake 2007; Podio 2003).

The nodal pressure relationship for a flow segment between two nodes with pressures $p_1$and p_2 may be expressed in (2.1):

$$p_2 = p_1 + \Delta p_h + \Delta p_f \quad (2.1)$$

where Δp_h is the hydrostatic pressure contribution and Δp_f is the frictional pressure losses along the flow path.

Frictional losses in wells and surface piping are commonly modeled using the Darcy–Weisbach equation as illustrated in (2.2):

$$\Delta p_f = f \frac{L}{D} \frac{\rho V^2}{2} \quad (2.2)$$

where f is the Darcy friction factor, L is the segment length, D is the internal diameter, ρ is the fluid density and V is the average flow velocity. The velocity is given by $V = Q/A$ for incompressible flow illustrating that

frictional pressure loss exhibits a quadratic relationship with volumetric flow rate Q (White 2015).

This quadratic behavior is often generalized using a lumped-parameter resistance formulation as expressed in (2.3):

$$\Delta p \approx R q^2 \quad (2.3)$$

where R represents a combined hydraulic resistance parameter capturing pipe geometry and relatively constant fluid properties (Palm 2013).

(Rowlan et al. 2009) demonstrated that the pump intake pressure (PIP) of a PCP well can be estimated from the surface casing-head pressure (CHP) and the hydrostatic head of the liquid column in the annulus under static annulus conditions. They also assumed negligible flow and friction in the casing annulus under normal PCP operating conditions. Due to the low annular velocities typically present during PCP systems production, this assumption is generally valid (Rowlan et al. 2009).

The differential (lift) pressure across the PCP is determined as the difference between the discharge pressure and the intake pressure. This represents the sole hydraulic load the pump must overcome (Lake 2007; Podio 2003). (Ceballos and Vivas 2019) connected this hydraulic load to measurable surface variables by expressing that the hydraulic torque T_h

developed by a PCP is proportional to the pump displacement per revolution and the differential pressure across the pump and is given by (2.4):

$$T_h = Cs\Delta p \quad (2.4)$$

where s is the pump displacement per revolution, Δp is the differential pressure and C is a unit-consistent proportionality constant.

The total torque measured at the surface T_{Total} comprises both hydraulic torque contribution and mechanical friction torque T_f. The friction torque term accounts for rotor to stator contact, elastomer deformation and surface drive-train losses. The equation for total torques is expressed in (2.5):

$$T_{Total} = T_h + T_f \quad (2.5)$$

Substituting the hydraulic torque relationship into the total torque equation produces an equation that links wellbore hydrostatics to the surface-measured torque. The updated equation for total torque is given in (2.6):

$$T_{Total} = (C \cdot s \cdot \Delta p) + T_f \quad (2.6)$$

The relationship between wellbore hydrostatics and surface-measured mechanical torque is essential for establishing the foundational nonlinear

measurement model required for virtual state estimation using the Extended Kalman Filter (EKF).

2.6 Kalman Filter Estimation

The foundation of modern state estimation for dynamic systems is rooted in the Kalman filter (KF). The KF was originally introduced by Kalman in 1960 as an optimal recursive estimator for linear systems that are subjected to Gaussian noise. The KF provides a minimum-variance unbiased estimate of unmeasured states by combining a mathematical system model with noisy measurements (Simon 2006).

In discrete-time form, a linear stochastic system is described by the state-space equations (2.7) and (2.8):

$$x_{k+1} = A_k x_k + B_k u_k + w_k \quad (2.7)$$

$$y_k = H_k x_k + v_k \quad (2.8)$$

where x_k is the state vector, u_k is the control input and y_k is the measurement vector. The process noise w_k and measurement noise v_k are assumed to be zero-mean Gaussian white noise processes with covariance matrices Q_k and R_k respectively (Simon 2006; Grewal and Andrews 2014).

The Kalman filter operates through a recursive predict–update structure. During the prediction step, the filter projects the state estimate and its associated covariance forward in time using the system model. In

the update step, model confidence is balanced against measurement uncertainty by the incorporation of incoming measurements via the Kalman gain (Welch and Bishop 2006).

While the standard KF is optimal for linear systems, many real-world engineering systems including artificial-lift well exhibit pronounced nonlinear behavior. In PCP systems, nonlinearities stem from quadratic friction losses, hydrostatic coupling, multiphase flow effects and electromechanical interactions between the pump and the motor. As a result, the linear Kalman filter is inadequate for accurate state estimation in these environments (Jazwinski 1970; Palm 2013).

To address nonlinear dynamics, the Extended Kalman Filter (EKF) was developed as a practical approximation to the nonlinear Bayesian estimation problem. The EKF applies a first-order Taylor series expansion to locally linearize the nonlinear state and measurement equations at each time step (Jazwinski 1970).

The nonlinear system is described by equations (2.9) and (2.10):

$$x_{k+1} = f(x_k, u_k) + w_k \quad (2.9)$$

$$y_k = h(x_k) + v_k \quad (2.10)$$

where f represents the nonlinear transition of states and h represents the nonlinear relationship between the states and the sensors (Simon 2006).

At each iteration the EKF computes the Jacobian matrices F_k and H_k using the equations (2.11) and (2.12):

$$F_k = \frac{\partial f}{\partial x}\Big|_{\hat{x}_k} \quad (2.11)$$

$$H_k = \frac{\partial h}{\partial x}\Big|_{\hat{x}_k} \quad (2.12)$$

which are used to propagate the error covariance and compute the Kalman gain (Grewal and Andrews 2014).

The EKF prediction step propagates the state estimate and covariance using the linearized system dynamics in equations (2.13) and (2.14):

$$\hat{x}_{k/k-1} = f\left(\hat{x}_{k-1}, u_{k-1}\right) \quad (2.13)$$

$$P_{k/k-1} = F_k P_{k-1} F_k^T + Q_k \quad (2.14)$$

During the update step, the innovation $y_k - h(\hat{x}_{k/k-1})$ is used to correct the prediction using equations (2.15) and (2.16):

$$K_k = P_{k/k-1} H_k^T ¿$$

$$\hat{x}_k = \hat{x}_{k/k-1} + K_k\left[y_k - h\left(\hat{x}_{k/k-1}\right)\right] \quad (2.16)$$

In finite-precision computing environments, the standard covariance update formulation may introduce numerical instability. A loss of symmetry or positive definiteness in the covariance matrix usually occurs as a result. The Joseph stabilized form provided in equation (2.17) is employed for

real-time observers deployed in industrial control systems to mitigate the risk of losing covariance matrix symmetry (Grewal and Andrews 2014).

$$P_k = (I - K_k H_k) P_{k/k-1}$$ ¿

The inherent inverse relationship between the physical fluid level in the annulus and the torque measured at the surface becomes highly sensitive to modeling errors when applying the EKF-based estimation to PCP systems (Rowlan et al. 2009; Ceballos and Vivas 2019). When submergence decreases, hydrostatic support diminishes resulting in an increase in the lift pressure and the hydraulic torque required by the motor.

The EKF is fundamentally an approximation therefore, unmodeled dynamics such as transient spikes in rotor-stator friction or sand production can cause the filter to diverge from the true state which results in estimation drift (Gelb 1974; Kouhi et al. 2020). A robust model and meticulous tuning of the process and measurement noise covariance matrices are required to balance the underlying physics against ambiguous surface measurements and mitigate the estimation drift.

3 Methodology

3.1 Existing System Overview

The existing Progressive Cavity Pump (PCP) installations at Company X's offshore locations are powered by a localized generator. The generator supplies three-phase power to the PCP induction motor via a Variable Frequency Drive (VFD). As illustrated in Figure 3 .3, the surface equipment which comprises of the surface drive, stuffing box and associated drive-train component is mounted directly at the wellhead, while the stator and rotor are installed subsurface at the end of the rod string. Pressure switches are installed on the location's hydraulic Emergency Shutdown (ESD) system and the Tubing Head Pressure (THP) flowline. The pressure switches are configured to automatically trip the VFD during abnormal low pressure events.

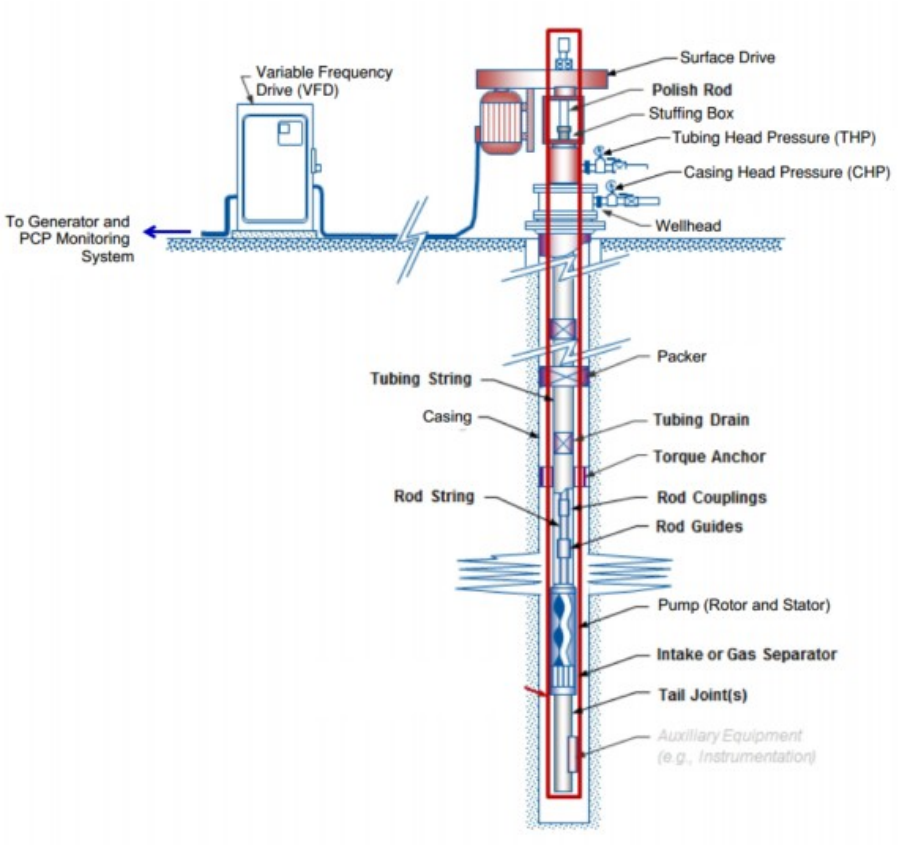

Figure 3.3: Surface and Subsurface components of a PCP system

The PCP monitoring and VFD telemetry are managed by a vendor's proprietary production optimization platform which aggregates surface drive data and provides operators with historical trending and fault detection. The vendor's system determines pump-off conditions by relying on temperature sensors. While exact proprietary algorithms are unknown, temperature-based pump-off detection typically functions by monitoring thermal spikes caused by severe elastomeric friction when the pump operates without fluid lubrication. Consequently, this method relies on a lagging indicator when the fluid level has already depleted and dry-running friction is actively occurring. Additionally, the system lacks the capability to

continuously calculate or monitor dynamic downhole fluid submergence prior to these thermal events.

Currently at PCP locations, the fluid submergence is verified using manual acoustic fluid shots once monthly. This method provides an inadequate snapshot of wellbore hydrodynamics that cannot support dynamic production optimization or rapid transient mitigation. Furthermore, the telemetry acquired by the proprietary controller is routed exclusively to a vendor-managed cloud architecture that requires the company to incur monthly Software-as-a-Service (SaaS) subscription fees to access the production data.

In parallel to the vendor's monitoring system, wellhead THP and CHP are measured via pressure transmitters hardwired directly to the analog inputs of a VolleyBoast (VoBo HL) IIoT endpoint. Additionally, the well location's hydraulic ESD pressure switch is wired to the discrete digital input of this IIoT endpoint. The VoBo HL transmits these facility parameters to the SCADA Human-Machine Interface (HMI) as described in 3.2 IIoT System Architecture, where supervisory safety logic evaluates the THP and CHP values against configured high and low-pressure alarm thresholds. With this existing architecture, engineers and operators must actively monitor two distinct interfaces to understand the status of a single well as shown in Figure 3 .4 and Figure 3 .5.

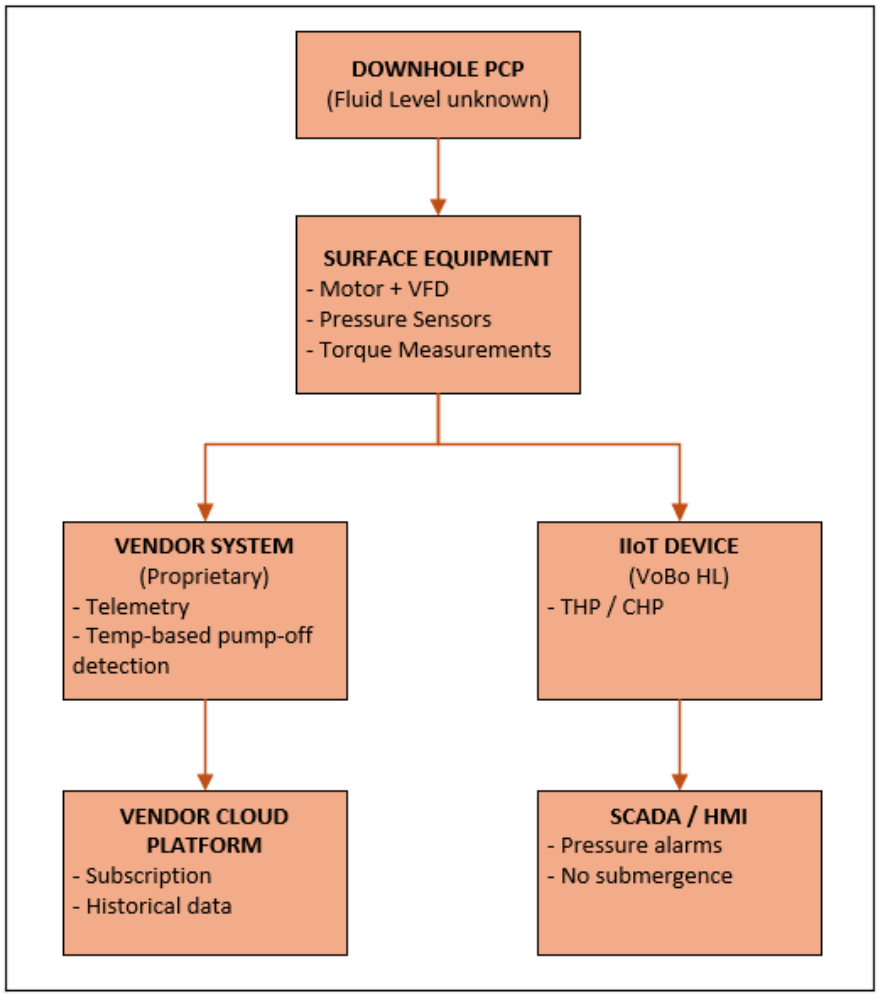

Figure 3.4: Block Diagram of Existing System

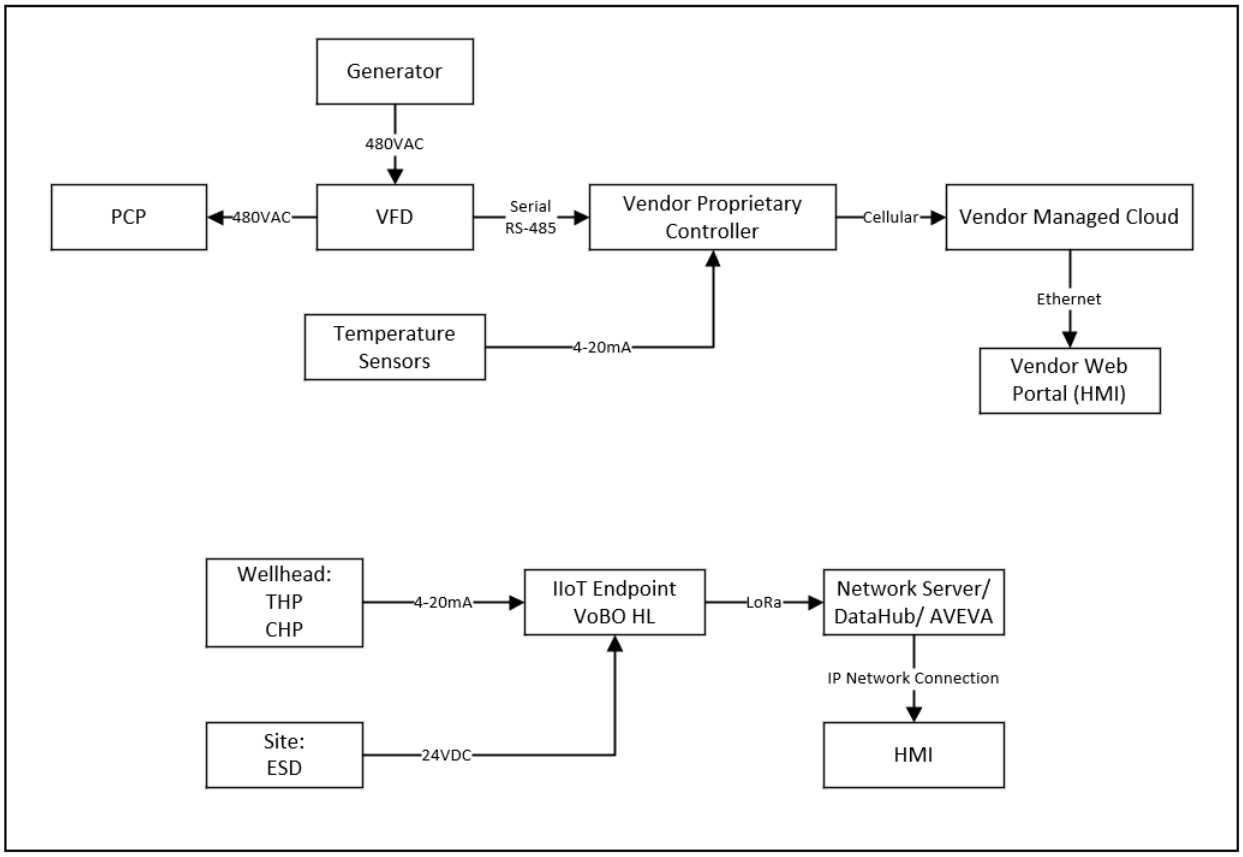

Figure 3.5: Existing System Functional Diagram

To resolve the limitations of this fragmented, reactive monitoring approach, the subsequent sections of this methodology detail the proposed IIoT architecture for the PCP system.

3.2 IIoT System Architecture

PCP data is collected using a VolleyBoast (VoBo HL) IIoT device installed at the well site. The IIoT device communicates with an ABB ACS800 VFD using a serial Modbus RS-485 interface. This connection facilitates real-time acquisition of key operating parameters such as motor speed, torque and current. Additionally, PCP CHP and THP are acquired by Murphy PXT-K transmitters connected to the wellhead casing and tubing

respectively and the analog inputs of the VoBo HL. These measurements are used in the estimation model.

The VoBo transmits these telemetry packets at five-minute intervals using a LoRaWAN (Long Range Wide Area Network) communication system to a nearby gateway. The packets are then forwarded to the ChirpStack network server where device authentication and decoding of the incoming payloads is executed before passing them to Cogent DataHub. The communication between ChirpStack, Cogent DataHub is facilitated using Message Queuing Telemetry Transport (MQTT) protocol. MQTT utilizes a publish–subscribe approach for data delivery.

Node-RED subscribes to Cogent DataHub at the same five minute cadence, using MQTT and executes the EKF algorithm whenever a complete telemetry packet is received. A web-based HMI dashboard was also developed using Node-RED. The features of this dashboard are detailed in Section 3.5.3 of this methodology.

In addition to the state estimation, supervisory intervention was configured where authorized operators can enter a new target motor speed in the Company's AVEVA HMI. The new setpoint is transmitted using MQTT to Cogent DataHub and subscribed to by Node-RED where it is formatted into Base64-encoded downlink payloads. Subsequently, the payloads are forwarded to the ChirpStack network server which schedules the LoRaWAN downlink transmission. Upon receiving the downlink, the VoBo HL writes the new speed reference to the ABB ACS 800 VFD via the Modbus RS-485 interface, thus completing the bidirectional IIoT control loop as illustrated in Figure 3 .6 and Figure 3 .7.

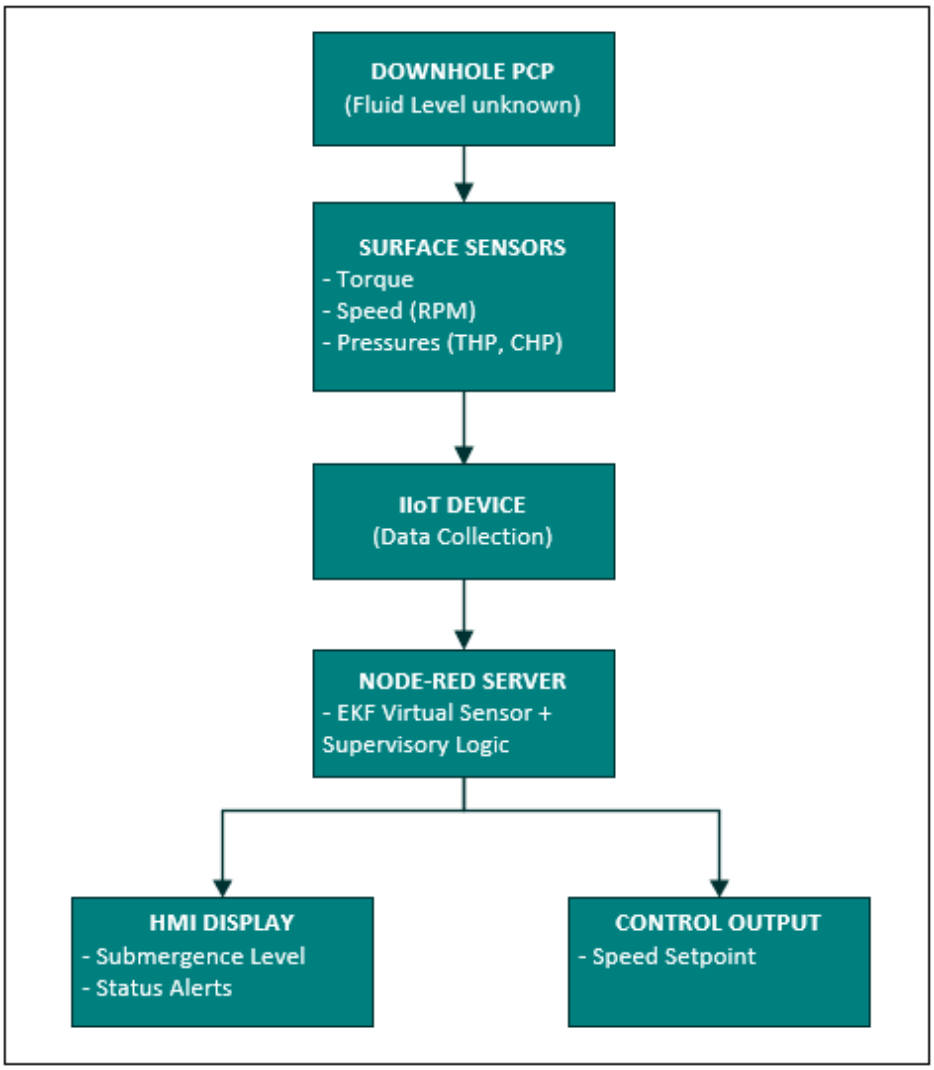

Figure 3.6: Block Diagram of the Proposed System

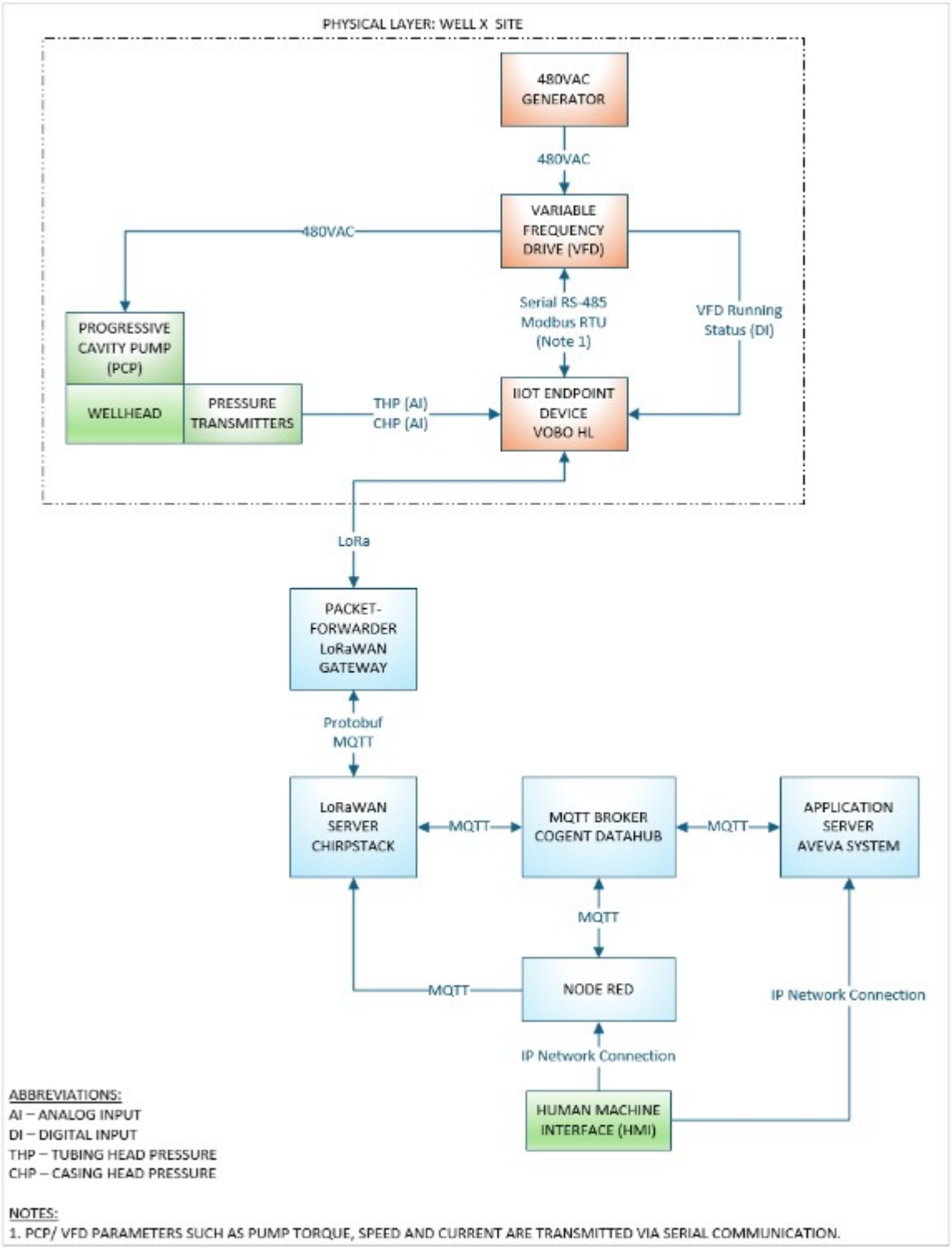

Figure 3.7: System Flow Diagram

3.3 PCP System Modeling

Based on the computational constraints of continuous IIoT execution outlined in the literature review, the dominant input–output behavior of the PCP system was modelled using a reduced-order state-space representation. The objective of this modeling phase was to maintain the essential physical relationships necessary for state observability without replicating the full multiphase complexity of the wellbore.

The discrete-time system state x_k is defined as the downhole fluid submergence which is not directly measurable using surface instrumentation. The system inputs comprise surface-measured variables including rotational speed, THP and CHP. The measured system output available to the observer is the mechanical surface torque.

Rotational speed is classified as a known system input since it is directly regulated by the ACS 800 VFD using Direct Torque Control and it does not independently contribute to the observability of the submergence state. Instead, the measured torque is selected as the primary measurement variable because of its direct relationship to the hydraulic load from the fluid above the pump intake.

3.3.1 Derivation of the Reduced-order Hydrostatic Model

A mathematical correlation between the unobservable downhole fluid PCP submergence and the measured torque is established to formulate the

state-space equations for the EKF. This process involves the mapping of the pressure differential across the PCP geometry.

3.3.1.1 Assumptions

1. The fluid within the tubing string is an incompressible liquid (oil/water mixture) due to the dominance of liquid-phase heavy oil in the production stream and the relatively low gas content during steady-state operation.

2. The gas interference within the tubing column is negligible thus, a constant linear fluid gradient ($Grad_{Liq}$).

3. The mechanical elasticity of the rod string remains constant and torsional slippage is neglected during steady-state operation due to the low SCADA telemetry sampling rate (5-minute intervals), which effectively acts as a low-pass filter.

3.3.1.2 Intake and Discharge Pressure Modelling

The intake pressure ($P_{\int ¿¿}$) at the pump suction is determined by the CHP combined with the hydrostatic pressure exerted by the annular fluid column. Let x_k represent the dynamic fluid submergence level, therefore, the intake pressure is given by equation (3.1):

$$P_{\int ¿ = CHP + (Grad_{Ann} \cdot x_k) \quad (3.1) ¿}$$

The discharge pressure (P_{dis}) at the pump outlet is a function of the THP, the total vertical depth of the well (D) and the dynamic friction losses within the tubing (ΔP_{fric}) and modelled in equation (3.2):

$$P_{dis} = THP + \left(Grad_{Liq} \cdot D \right) + \Delta P_{fric} \quad (3.2)$$

3.3.1.3 Friction Modelling

The dynamic friction loss (ΔP_{fric}) is non-linearly proportional to the square of the volumetric flow rate (Q). Given that the flow rate of a positive displacement pump is directly proportional to its rotational speed (ω) multiplied by a geometric pump constant (K_Q), the friction can be modeled as:

$$\Delta P_{fric} = K_F \cdot \left(K_Q \cdot \omega \right)^2 \quad (3.3)$$

where K_F is the dynamic friction coefficient.

3.3.1.4 Differential Pressure and Torque Mapping

The total differential pressure (ΔP) across the PCP stator is defined in equation (3.4):

$$\Delta P = P_{dis} - P_{\int} \quad (3.4)$$

The total mechanical torque required at the surface (T_{calc}) to overcome this differential pressure consists of the hydraulic torque and the lumped

mechanical frictional losses of the system (τ_0) is given by equation (3.5), where the pump's specific torque constant is K_T.

$$T_{calc} = K_T \cdot (\Delta P) + \tau_0 \quad (3.5)$$

Substituting equation (3.4) into (3.5):

$$T_{calc} = K_T \cdot ¿$$

Substituting equations (3.1) and (3.2) into (3.6):

$$T_{calc} = K_T \cdot \left(\left[THP + \left(Grad_{Liq} \cdot D \right) + K_F \cdot \left(K_Q \cdot \omega \right)^2 \right] - \left[CHP + \left(Grad_{Ann} \cdot x_k \right) \right] \right) + \tau_0 \quad (3.7)$$

This derived equation establishes a connection between the system's measurable inputs (THP, CHP, ω), the unobservable state (x_k) and the torque measurement (T_{calc}). This serves as the foundation for the EKF measurement-update vector $h¿$.

Additionally, equation (3.7) illustrates a nonlinear physical system where dynamic friction losses in the tubing ΔP_{fric} exhibits a quadratic relationship with the pump’s volumetric flow rate Q^2. Consequently, there is a nonlinear mapping between the unobservable system state and the measured surface torque rendering the standard Kalman filter formulation unsuitable. Therefore, a nonlinear stochastic observer is required for maintain accurate estimations across varying operating conditions. The Extended Kalman Filter is utilized to locally linearize the measurement function around the current state estimate, facilitating efficient real-time estimations that are suitable for IIoT deployment.

3.4 Extended Kalman Filter (EKF) Formulation

3.4.1 EKF Definitions

The EKF is designed as a one-dimensional observer using submergence as the only unobservable state required for supervisory control. All other variables are either measured or classified as known inputs. The submergence slowly changes relative to the telemetry update rate, as a result, the state dynamics are modeled as a stochastic random walk (change) given by the equation (3.5):

$$x_k = x_{k-1} + w_{k-1}, w_{k-1} \sim N(0, Q) \quad (3.5)$$

where x_k is the downhole fluid submergence and w_{k-1} is the process noise term that models the unmeasured disturbances affecting submergence and is defined as Gaussian (normal) distribution with zero mean with covariance Q.

The measured torque is selected as the only corrective measurement as illustrated in (3.6). This is due to its dominant and direct observability relationship with submergence:

$$z_k = \left[T_{meas,k} \right] \quad (3.6)$$

3.4.2 EKF Prediction

The prediction step propagates the state estimate and associated covariance forward in time and is given by equations (3.7) and (3.8):

$$\hat{x}_k^- = \hat{x}_{k-1} \quad (3.7)$$

$$P_k^- = P_{k-1} + Q \quad (3.8)$$

where $\hat{x}_k^-$ is the predicted state estimate and P_k^- is the predicted estimation error covariance. The covariance term P_k represents the uncertainty in the state estimate.

3.4.3 EKF Correction

The correction step updates the predicted state using measured surface torque. Given the predicted submergence estimate $\hat{x}_k^-$, the nonlinear measurement function is first evaluated to compute the expected surface torque h provided by the current state estimate and measured operating conditions using equation (3.9):

$$h$$

The equation represents the surface torque expected to be observed if the predicted submergence $\hat{x}_k^-$ was correct. The innovation or measurement residual ν_k is then computed in equation (3.10) as the difference between the measured surface torque z_k and the expected torque. An increase in submergence correlates with a positive innovation whereas a negative innovation is indicative of decreased submergence.

$$\nu_k = z_k - h$$

The EKF linearizes the measurement model at each prediction. The measurement Jacobian H_k is therefore given by equation (3.11):

$$H_k = \frac{\partial h}{\partial x} \Big|_{\hat{x}_k^-} \quad (3.11)$$

Substituting the measurement function and differentiating with respect to submergence yields equation (3.12):

$$H_k = -K_T \cdot Grad_{Ann} \quad (3.12)$$

The Jacobian defines the sensitivity of surface torque to submergence. The negative sign indicates that increasing submergence increases pump intake pressure which decreases the pressure differential across the pump and consequently reduces the required surface torque.

The Kalman Gain balances confidence between the model and the measurements. Larger gains prioritize measurements whereas smaller gains prioritize the model prediction. The Kalman Gain K_k is then computed by equation (3.13):

$$K_k = P_k^- H_k^T$$

The predicted submergence estimate is then updated proportionally based on the observed torque discrepancy and scaled by the Kalman Gain and is given by (3.14):

$$\hat{x}_k = \hat{x}_k^- + K_k \nu_k \quad (3.14)$$

Following the state update, the estimation error covariance P_k is updated to reflect the increased confidence in the corrected estimate using the Joseph stabilized covariance update form given by equation (3.15). This update is required to maintain numerical stability and align physics-based predictions with real-time surface measurements during extended real-time execution thereby enabling accurate and stable estimation of the downhole submergence by preventing unrealistic confidence in filter updates.

$$P_k=(I-K_k H_k)\ P_k^{¿\,¿¿}$$

The first term illustrates the reduction in uncertainty from measurement information while the second term addresses the measurement noise uncertainty.

3.4.4 EKF Model Parameters

The well depth (D) and PCP well pressures $(CHP \wedge THP)$ were obtained from well completion records and field instrumentation respectively. The pressure gradients in the tubing and annulus $(Grad_{Liq} \wedge Grad_{Ann})$ were classified as average hydrostatic pressure contributions from the produced fluid columns. These were calibrated using observed pressure behaviour during stable operating conditions, aligning with the reduced-order modelling approach used in Section 3.3.1. The pump-specific coefficients $(K¿¿Q, K_T)¿$ and mechanical loss terms $(K¿¿F, \tau_0)¿$ were also established

using manufacturer specifications and then adjusted by analyzing steady-state torque telemetry.

The filter's transient responsiveness and noise-rejection characteristics are governed by the process (Q) and measurement (R) noise covariances. The measurement noise covariance reflects the statistical confidence in the physical surface torque sensor and was quantified by calculating the variance of torque readings during a stable pumping period. This baseline effectively constrains the estimator's sensitivity to electrical and mechanical noise.

With the measurement noise fixed, the process noise covariance was iteratively tuned offline using historical telemetry replays. Adjustments were made until the innovation (residual error) ν_k residual error centered around zero, exhibiting no predictable repeating pattern during steady-state operations. This process confirmed that the virtual sensor was optimized without mathematical bias, rendering it suitable for live IIoT deployment.

3.5 System Implementation and Supervisory Control

3.5.1 EKF Constraint Mechanisms

The EKF algorithm is deployed in Node-RED on a centralized server. The mathematical foundation of the EKF assumes that system noise is standard and predictable (Gaussian). However, in real-world applications, PCP systems frequently encounter unpredictable disturbances such as gas

ingress or high-viscosity slugs. To mitigate model instability, the following constraints were used as safeguards independent of the EKF calculations:

- **Pump State Interlock:** The pump status is evaluated before each estimation cycle. If a digital offline flag (VFD not running) is detected, the measurement-update phase is bypassed. This avoids artificial state collapse from near-zero torque readings and preserves the estimate.
- **State Correction Rate Limit:** The response to torque spikes is limited by a drawdown cap of 15.2 m/min (50ft/min). This specific threshold was established through an iterative, offline tuning process that utilized historical telemetry replays. This optimized limit serves as a shock absorber ensuring that the model remains within hydrostatic limits while effectively tracking real drawdown trends.
- **Friction Torque Interlock:** A pump-off condition or loss of hydrostatic load is indicated when surface torque approaches the base mechanical friction (τ_0). During pump-off, gas replaces the fluid column which violates the model assumption of liquid-filled tubing. An unconstrained EKF will attempt to inflate the fluid level estimate to match the low measured torque. To prevent this, supervisory logic overrides the observer to set the submergence to zero and changes the dashboard Submergence status to a "Pump-Off" condition.

3.5.2 Supervisory Speed Control Strategy

Automated speed modulation was intentionally excluded from the deployed architecture. This was due to the high mechanical risk of rod-string failure during transient flow events. Alternatively, the system functions as a human-in-the-loop supervisory controller. Alerts are generated for the operator to review when conditions like low submergence occur.

Authorized speed adjustments are entered through the Company's restricted-access AVEVA SCADA HMI. The SCADA system transmits the setpoint via MQTT which is subscribed to by Node-RED. These setpoints are then scaled, converted to Base64-encoded command payloads and scheduled for transmission through the ChirpStack LoRaWAN network server to the designated target VoBo HL's Device EUI, thus completing the bidirectional control loop.

3.5.3 Operator Interface Design

An HMI dashboard was developed within the Node-RED environment to bridge the computational back-end with field operations by dynamically parsing incoming MQTT JSON payloads and displaying them in real-time. It aggregates decoupled PCP surface measurements such as RPM, casing pressure, tubing pressure and torque. The dashboard also facilitates the option to simultaneously trend selected PCP measurements along with the unobservable downhole state estimates generated by the EKF. Additionally,

the HMI dynamic status indicators shift deterministically between operational states (e.g., Normal, Anomaly, Offline or Pump-Off) based on the underlying algorithmic safeguards.

The HMI was also designed with a restricted, password-protected "Debug Mode" to serve as a localized computational sandbox and calibration interface. This module permits the upload and injection of historical, CSV telemetry logs directly into the Node-RED computational backend where submergence values and PCP parameters can be observed on the dashboard and trended as logs are computed every second, similar to the five-minute cadence in the live mode.

The debug interface also allows authorized users to inject updated physical parameters (such as wellbore depth, $Grad_{Liq}$ or τ_0) and tuning variables $(Q \wedge R)$ directly into the Node-RED computational backend. Consequently, the observer can be re-tuned and calibrated, in response to changing reservoir conditions, eliminating the need for source-code modifications.

3.6 Testing and Evaluation

The evaluation was divided into two distinct phases, the empirical validation of the EKF virtual sensor and the bench testing of the active closed loop speed control pathway.

3.6.1 Virtual Sensor Validation

The performance of the EKF state estimator was evaluated across a spectrum of operational conditions to validate its theoretical formulation against practical field dynamics. The testing framework defined three validation scenarios and the outcomes are discussed in Section 4:

1. **Steady-State:** This scenario evaluates the estimator's stability and noise-rejection capabilities and covariance tuning during stable VFD operation. If the process noise covariance (Q) and measurement noise covariance (R) are optimally tuned, the measurement innovation (v_k) should be uncorrelated and unpredictable.

   During this phase, the Node-RED dashboard should continuously reflect a "Normal" operational status. The submergence gauge should stabilize and closely track the manual acoustic fluid level measurement.

   The estimator’s accuracy was also established by comparing its submergence estimates against independent, acoustic fluid-level shots and quantified using the Root Mean Square Error (RMSE). RMSE was selected over alternative metrics such as Mean Absolute Error (MAE) or Mean Absolute Percentage Error (MAPE) to align with both the observer’s mathematical formulation. The EKF is a minimum-variance estimator designed to minimize the mean square estimation error thus

RMSE is the most theoretically consistent performance metric. Furthermore, the RMSE squares the residuals thus disproportionately penalizing the large estimation outliers.

2. **Pump off Simulation:** This scenario evaluates the deterministic friction torque interlock described in section 3.5.1. The induction of a pump-off event on a live, producing PCP risks catastrophic elastomeric stator failure, hence this condition was validated using historical pump-off telemetry injected into the EKF simulator using the “Debug Mode” described in section 3.5.3. This scenario evaluates the supervisory logic to detect a pump-off condition and recognize when the measured torque converges toward the base mechanical friction boundary $(T_{meas} \leq \tau_0)$. The logic must successfully pre-empt the EKF measurement-update phase and clamp the submergence estimate to zero $(\hat{x} \¿ \¿ k \rightarrow 0) \¿$before mathematical divergence occurs with false mathematically inflated fluid levels.

   When the torque boundary is violated, the Node-RED dashboard must override the standard estimation display. The submergence value should be forced to 0 m (0 ft) and its status should display a critical "Pump-Off" status with visual red state indicators to alert the operator.

3. **Transient Disturbance:** This scenario assesses the observer's ability to maintain observability and re-converge following severe system disruptions, specifically scheduled pump shutdowns and subsequent restarts.

   The success is defined by the ability to maintain a bounded estimation error covariance (P_k) during the unobservable zero-speed period via the pump-state interlock described in section 3.5.1. Upon restart, the filter must process the initial high magnitude innovations without numerical divergence and re-converge to the true steady state fluid level.

   When the VFD shuts down, the dashboard should immediately transition the submergence status to "Offline" and freeze the submergence value to prevent estimation drift. Upon restart, as the PCP overcomes static friction, it is expected that the innovation bounds may be temporarily violated. The dashboard should log these violations and transition to an "Anomaly" status. The HMI submergence status should automatically clear the anomaly and return to the "Normal" state when the transient hydrodynamics settle and the EKF re-converges.

3.6.2 Closed loop Speed Control (Bench-test)

Bench-testing in a controlled workshop environment was initially executed to validate the control logic without risk to a live production asset.

The complete actuation pathway was deployed on an identical VFD and induction motor assembly. For this evaluation, target speed values were injected directly via the Node-RED interface and the payload translation was verified. Accuracy of the translation was validated via comparison with the Base64-encoded Modbus payloads generated by the official VolleyBoast Payload Configurator tool prior to being forwarded to the ChirpStack network server.

The LoRaWAN transmission cadence was accelerated to a 1-minute interval to evaluate system latency. The bench test successfully traced the command propagation from Node-RED, through the downlink scheduling via ChirpStack and finally to the Modbus RS-485 write-execution at the VoBo HL endpoint. End-to-end command latency was evaluated and validated on the VFD local display within the 1-minute transmission window.

3.6.3 Open loop Validation of Speed Control

While bench-testing successfully validated the hardware execution using forced inputs via Node-RED, the final solution requires that all target motor speed commands are entered via the Company’s AVEVA HMI. The company mandated that this feature must be tested in its finalized configuration due to the associated risks and the significant resources involved; approval was not granted for conducting the test more than once. However, at the time of this system evaluation, company resources were

unavailable to integrate the target speed input function into the AVEVA SCADA HMI. Consequently, to evaluate this software pathway without endangering the live, producing asset, an open loop validation methodology was designed.

In this open loop configuration, the end-to-end software integration was tested but the final communication link transmitting the downlink payload to the ChirpStack network server is intentionally disconnected thereby completely isolating the live offshore PCP from mechanical risk. The validation methodology traces the command sequence where a target motor speed (in RPM) is entered by an authorized operator into the back-end of the AVEVA system. This input is then transmitted via MQTT to the Cogent DataHub. Subsequently, Node-RED subscribes to this topic, scales the RPM to the corresponding Modbus integer and packages the JSON and generates the requisite Base64 string.

3.6.4 Closed Loop Speed Control Live Commissioning (Future)

The live deployment of the closed loop speed control on a producing asset was deferred pending the aforementioned HMI integration and therefore remains a future objective. Beyond the completion of the AVEVA SCADA interface, the transition to live actuation is contingent upon the completion of a formal risk assessment. Inducing speed transients on an active PCP poses mechanical risks, including torsional stress and potential

rod-string failure. Consequently, specific prerequisites must be met before live speed commands can be issued:

1. **Implementation of Additional Controls:** The development and integration of supplementary hardware and software safety interlocks to constrain allowable speed-change step sizes and enforce dynamic torque limits.

2. **On-Site Visual Verification**: As a mandatory precaution during initial closed loop commissioning, personnel must be deployed to the well site to ensure local, visual verification of the drive response when remote speed commands are issued. Additionally, personnel would provide an immediate manual override if required.

3.6.5 Offline Computational Analysis (MATLAB)

While the Node-RED dashboard facilitated real-time operational monitoring, quantitative evaluation of the virtual sensor was conducted offline using MATLAB. The SCADA telemetry and the corresponding EKF state outputs were exported as comma-separated values (CSV) logs. MATLAB plots were developed for each of the three validation scenarios (Steady-State, Transient Disturbance and Pump-Off Simulation). Additionally, a plot was generated for EKF submergence estimates against the acoustic fluid level measurements. Futhermore, MATLAB was used to mathematically verify that the estimator remains stable and successfully recovers from sudden operational disruptions. This was demonstrated by

plotting the measurement innovations (v_k) to confirm that they safely return to within the established ±203.4 Nm (±150 ft-lbs) confidence bounds. The ±203.4 Nm (±150 ft-lbs) confidence bound was mathematically established by analyzing the baseline statistical variance of the surface torque sensor during known steady-state operations.

Table 3.2: Summary of Testing and Evaluation

Operational Scenario	**Evaluation Criteria and Objectives**	**Expected Outcome / HMI Response**
Steady-State	• Validate baseline stability and noise-rejection. • Innovation (v_k) must be uncorrelated and unpredictable. • Accuracy benchmarked against acoustic shots using RMSE.	• Submergence values stabilizes and tracks acoustic baseline. • Submergence status continuously displays "Normal."
Transient Response	• Assess covariance (P_k) bounding during zero-speed unobservability. • Evaluate filter re-convergence following high-magnitude startup transients.	• Submergence status transitions to "Offline" during shutdown. • Startup transients log an "Anomaly" before clearing back to "Normal" upon re-convergence.
Pump-off Simulation	• Validate deterministic friction torque interlock ($T_{meas} \leq \tau_0$) using historical telemetry injected into the Node-Red “Debug Mode” simulator.	• Standard EKF update is pre-empted. • Submergence is clamped to 0 m (0 ft). • "Pump-Off" visual alert is triggered.
Bench Test Speed Control	• Validate hardware execution, network routing and latency using forced inputs via Node-RED on an identical workshop VFD assembly.	• Node-RED payloads mathematically match the VolleyBoast Configurator benchmark. • Successful RPM modulation verified on VFD display.
Open loop Speed Control	• Validate end-to-end software integration from AVEVA through Base64 payload generation. • Final MQTT downlink to ChirpStack is intentionally	• Successful protocol translation entirely in software. • Full execution deferred pending IT resource availability and risk

Operational Scenario	Evaluation Criteria and Objectives	Expected Outcome / HMI Response
	severed to protect the active asset.	assessment.
Live Commissioning (Future)	• Complete operational risk assessment, program dynamic torque interlocks, finalize AVEVA configuration and schedule on-site visual verification.	• Authorized, end-to-end live speed modulation executing on the offshore asset.

4 Results and Discussion

4.1 Evaluation Scenarios and Experimental Setup

The performance of the virtual sensor and supervisory control framework was evaluated through a structured series of operational scenarios specifically designed to assess state estimation accuracy, estimator stability, observability limitations and hybrid control performance in a live PCP system.

These experimental scenarios aimed to evaluate the EKF performance under steady excitation, loss of observability, model mismatch and hybrid constraint enforcement. All scenarios were executed using the Node-RED dashboard operating either in live mode or simulation mode using historical data depending on the associated operational risk. This architecture facilitated the integration of deterministic supervisory logic with EKF’s mathematical predictions thereby establishing a hybrid control system suitable for field deployment.

4.2 Well Profile and Baseline Initialization

The architecture was deployed using live SCADA telemetry from an operating production asset called “Well X”, to validate both the theoretical accuracy and practical robustness of the EKF-based virtual sensor. Well X is a PCP installation located offshore in the southwest region of Trinidad and was drilled and completed at vertical depth of 1,420.4 m (4,660 ft). Laboratory fluid analysis of the produced multiphase mixture confirms that Well X contains a heavy crude oil with an API gravity that ranges between 9.0° and 10.0° at 15.6°C (60°F). The multiphase fluid is characterized by a highly variable total water content, measured between 7.9% and 75.2% by volume and demonstrates a viscosity ranging between 6,725 cP at 48.9°C (120°F) and to 84,100 cP at 30.0°C (86°F).

The Node-RED program was initialized using the following baseline parameters:

- Volumetric Pump Constant (K_Q): 4.107
- Torque Constant (K_T): 0.30
- Friction Coefficient (K_F): 0.001
- Base Mechanical Friction (τ_0): 115.2 Nm (85 ft-lbs)
- Annular Gas Gradient $(Grad_{Ann})$: 0.06 psi/ft

During a stabilized operating interval, the pump operated at a speed of 59 RPM and a measured torque of 559 ft-lbs. An acoustic fluid level shot was conducted and indicated a dynamic fluid submergence x_k of approximately 381.0 m (1,250 ft). The substitution of these measured values into the hydraulic-mechanical torque model determined that the tubing fluid gradient ($Grad_{Liq}$) was 0.34 psi/ft. This calibration established a reliable baseline and ensured that the EKF commenced estimation from a validated operating point.

4.3 Steady-State Estimation

The stability of the EKF was evaluated under continuous, steady-state conditions using telemetry from Well X. The evaluation was conducted on data captured via Node-RED between 29 April 2026 and 4 May 2026. Plots were generated using MATLAB as illustrated in Figure 4 .8, demonstrating that the virtual sensor effectively tracks the unmeasured downhole fluid submergence state without exhibiting signs of mathematical divergence.

During this evaluation period, the surface torque and wellhead pressures demonstrated stability and the innovation of the estimator remained consistently near zero. These findings confirm that the covariance matrices for process noise Q and measurement noise R have been appropriately scaled and a steady-state solution was approached. Additionally, evidence of the observer's consistency with statistical design assumptions was evident in this evaluation. The live Node-RED dashboard

also displayed a “Normal” operational status throughout the period as shown in Figure 4 .9.

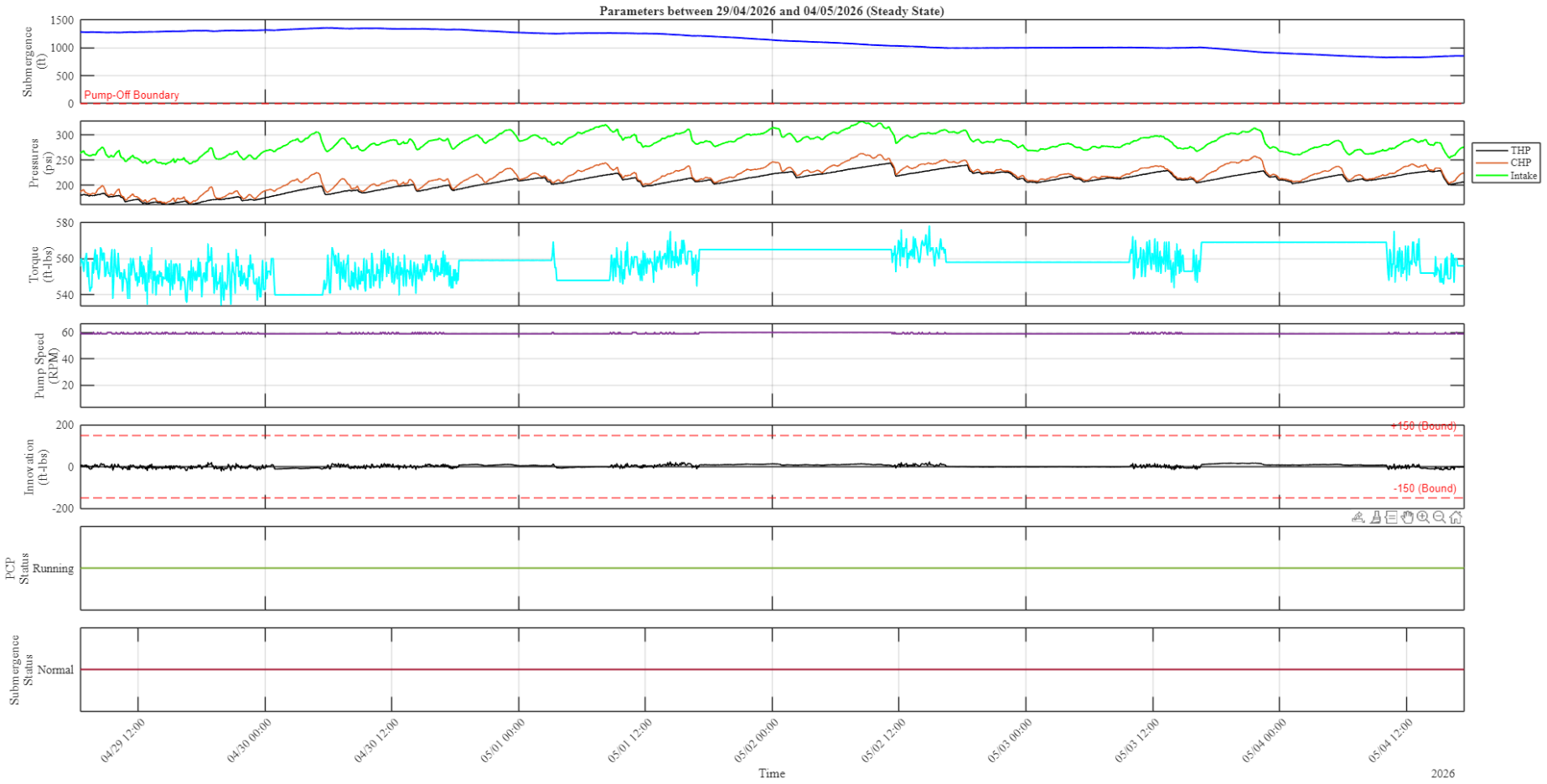

Figure 4.8: Plot of steady state parameters between 29 April 2026 and 4 May 2026

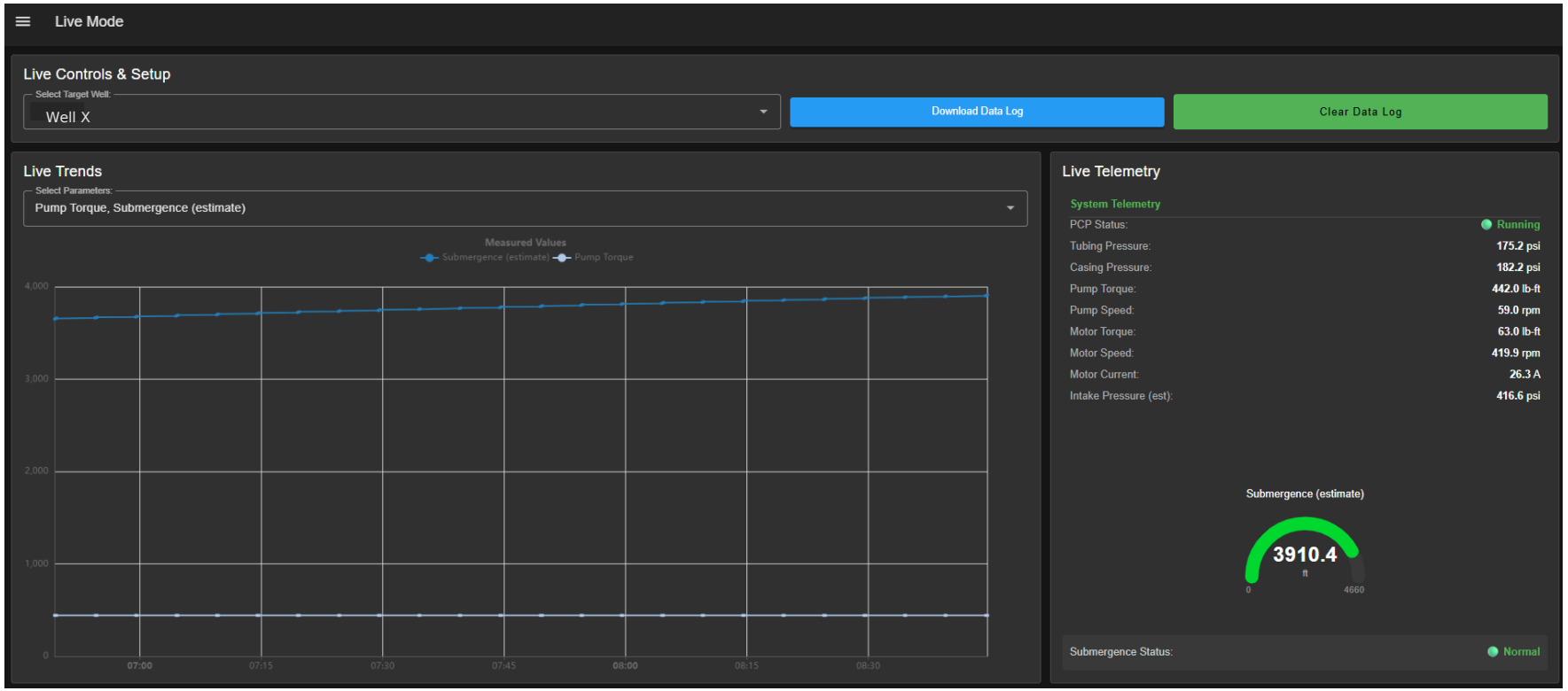

Figure 4.9: Screen shot of Node-Red Live Dashboard illustrating Normal operations

The accuracy of the converged state was assessed by comparing the EKF submergence estimates with independent downhole acoustic shots obtained during steady-state operations on select days as shown in Table 4 .3.

Table 4.3: Comparison between Acoustic shot and EKF estimate submergence levels

Date	Submergence Acoustic Shot (m) *(ft)*	Submergence EKF Estimate (m) *(ft)*	Error (m) *(ft)*
09 Apr 2026	356.3 *(1169)*	442.4 *(1452)*	+86.3 *(+283)*
13 Apr 2026	351.1 *(1152)*	425.5 *(1396)*	+74.4 *(+244)*
16 Apr 2026	356.3 *(1169)*	376.9 *(1237)*	+20.7 *(+68)*
21 Apr 2026	370.6 *(1216)*	399.6 *(1311)*	+29.0 *(+95)*
28 Apr 2026	379.8 *(1246)*	391.4 *(1284)*	+11.6 *(+38)*
07 May 2026	986.3 *(3236)*	928.7 *(3047)*	−57.6 *(−189)*

On May 7, following an extended shutdown and subsequent restart of the PCP, the estimator exhibited noteworthy performance when the fluid level experienced a significant transient recovery, rising from approximately 365.8 m (1,200 ft) to 986.3 m (3,236 ft). This capability to maintain accurate state tracking amid minor disturbances and throughout a dynamic recovery of 620.5 m (2,000 ft) underscores the effectiveness of the observer's physical state-space formulation across the wellbore.

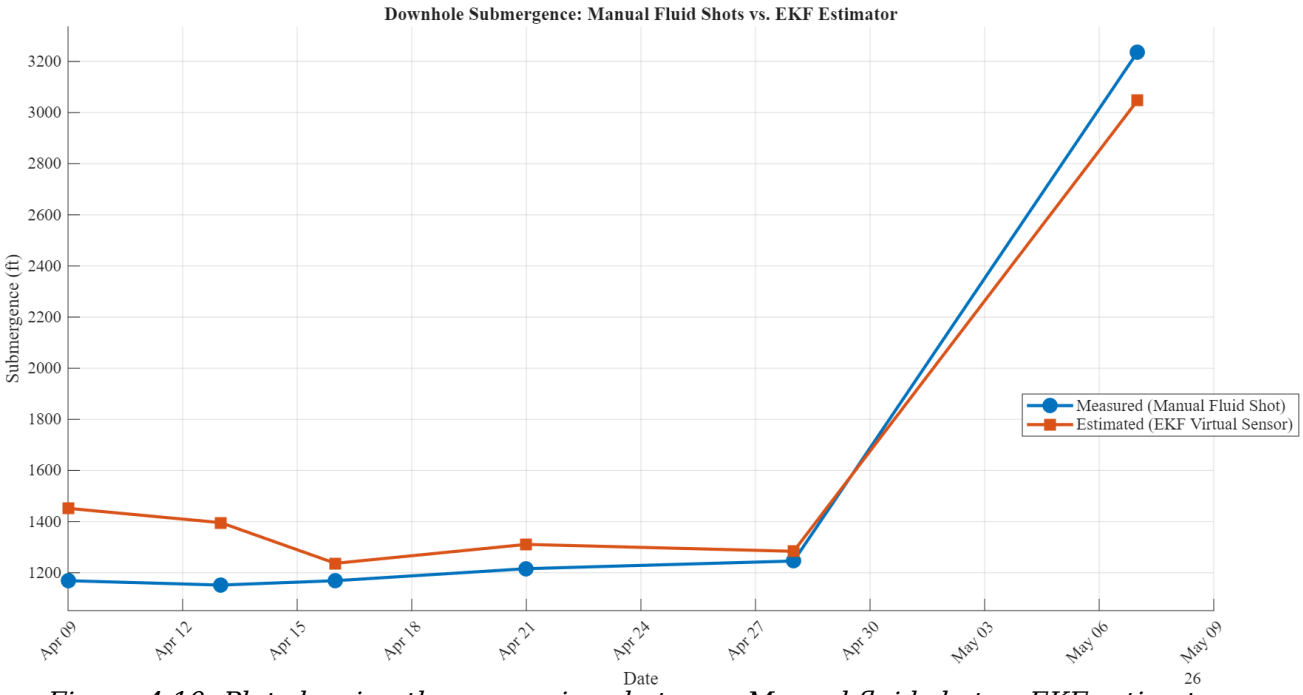

Figure 4.10: Plot showing the comparison between Manual fluid shot vs EKF estimate Submergence levels

Furthermore, the performance of the estimator was evaluated using the Root Mean Square Error (RMSE) calculated across the sample set. This resulted in an overall error of 54.3 m (178.2 ft). Given the total well depth of 1,420.6 m (4,660 ft), this RMSE translates to an error margin of 3.82% proving that a nonlinear observer can achieve significant accuracy using surface measurements only. Currently, there is no direct benchmark in the literature to compare this error metric against. From the literature review, it was observed that previous research into PCP submergence optimization relied on physical downhole sensors, surface flowmeters or mathematical simulations without field validation. Surface flowmeters are known to be unreliable in heavy oil. Therefore, this project establishes a new baseline for sensorless EKF submergence estimation on an active well using only surface measurements. A 3.82% error is acceptable and successfully meets

the operational requirements for the PCP control system because of the following reasons:

- **Pump-Off Prevention Buffer:** The main goal of the virtual sensor is to prevent the fluid level from dropping to the pump intake (0 m or 0 ft). An error of 54.3 m (178.2 ft) is small enough when a well is operating at safe submergence levels, such as above 304.8 m (1,000 ft). This error margin provides the system with enough time to detect a drawdown trend and activate the pump-off interlocks before the pump runs dry.
- **Acoustic Shot Accuracy:** The EKF estimates were compared against manual acoustic fluid-level shots to calculate the error. It is known that acoustic measurements have some degree of error, especially in heavy-oil wells due to gas interference and annular foam. Therefore, a portion of the 54.3 m (178.2 ft) error can be attributed to the acoustic baseline itself rather than the EKF model only.
- **Improvement over Lagging Indicators:** Previously, the only automated protection for a pump-off event was a temperature sensor. This sensor would trip the VFD only after the pump had already started running dry and heating up. The EKF model improves this reactive temperature sensor with a continuous submergence estimate that has an accuracy of over 96%.

The error can be attributed to the following factors within the model:

- **Static Parameter Approximation:** Key parameters such as the tubing fluid gradient ($Grad_{Liq}$) and mechanical friction (τ_0) are treated as constants. In reality, these parameters can vary with factors such as temperature, water cut and fluid composition. Any discrepancies in these assumed values introduces a systematic offset in pressure estimation. This ultimately leads to submergence estimation errors.
- **Simplified Friction Model**: The friction term used in the model is based on a quadratic relationship with the flow rate. It does not account for complex effects such as multiphase slip or changes in fluid viscosity thereby leading to often overestimation of frictional pressure losses, resulting in inflated torque predictions and consequently higher inferred submergence.

4.4 Simulated Pump-Off Condition

Directly inducing a pump-off event on a producing PCP system is operationally prohibited due to the high risk of irreversible stator damage. Therefore, a pump-off condition was evaluated using historical telemetry data injected into the EKF via the Node-RED simulator. Figure 4 .11 illustrates the resulting estimator response and measured parameters during this fault condition.

As annular fluid drawdown progressed, the EKF effectively translated the increasing surface torque into a declining submergence estimate. A critical event occurred when the fluid level in the annulus dropped below

the physical depth of the pump's intake resulting in the torque dropping abruptly to the mechanical friction limit τ_0. This event represents a violation of the model assumption of a fully liquid-filled tubing column. Under these conditions, the EKF encounters a pump-off paradox and erroneously increases the estimated fluid level in a mathematical effort to reconcile the suddenly low measured torque with its internal state equations.

The results demonstrate that the implemented friction torque interlock successfully addresses this failure mode. When measured torque convergence toward τ_0, the supervisory logic deterministically overrides the EKF estimates, sets the submergence estimate to zero and forces an immediate transition to a “Pump-Off” state displayed on the Node-RED dashboard and illustrated in Figure 4 .12.

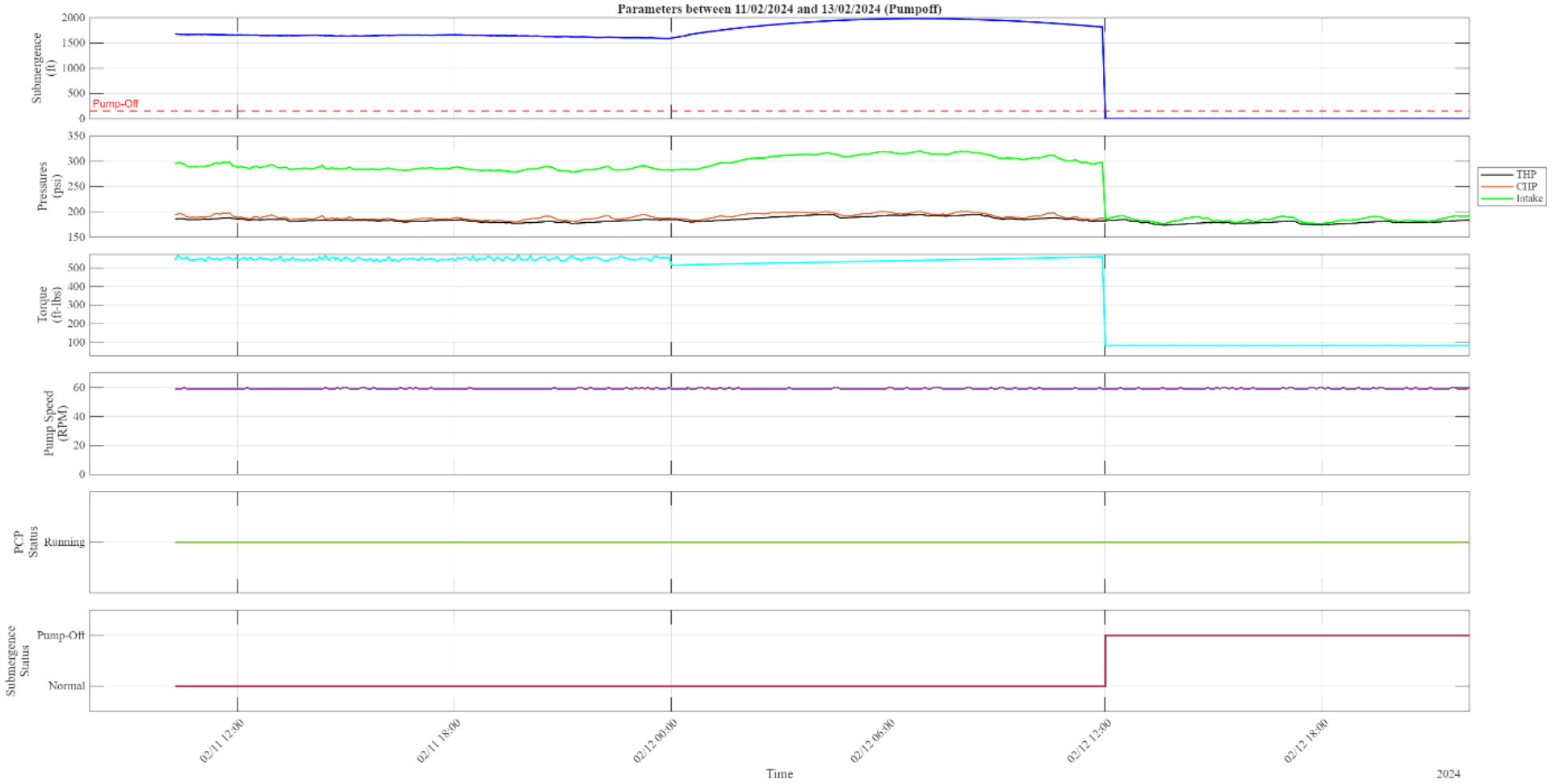

Figure 4.11: Plot of pump-off parameters between 11 February 2024 and 13 February 2024

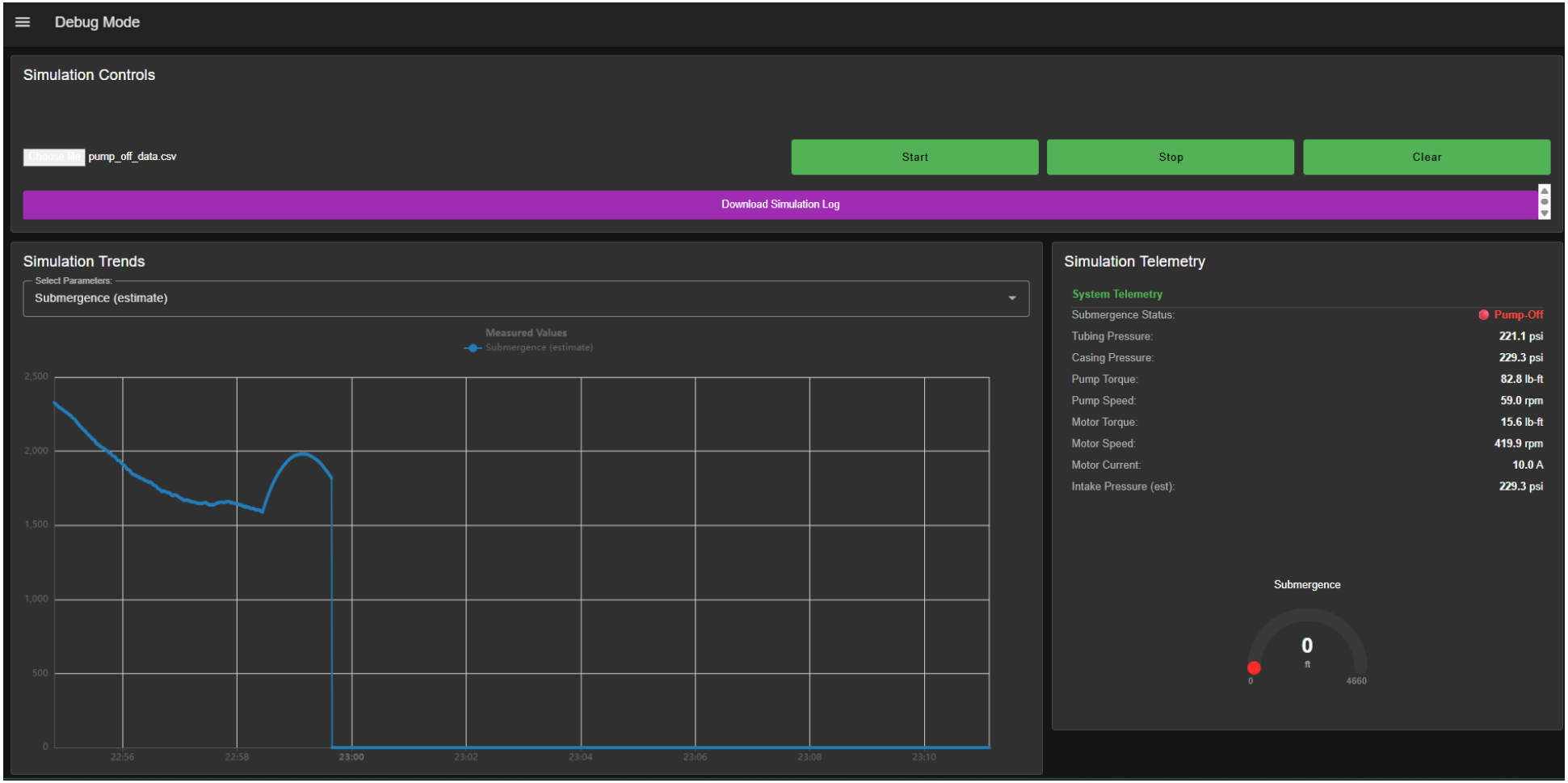

Figure 4.12: Dashboard screenshot illustrating a pump-off condition

4.5 Transient Response: Pump Shutdown and Restart

A shutdown and restart sequence for the PCP was analyzed using telemetry data recorded between March 30 and April 4, 2026. This analysis successfully evaluated the robustness of the estimator under transient disturbances, a loss of excitation (zero-speed) scenario and unstable fluid flow (see Figure 4 .13). On March 31, 2026, routine generator maintenance at Well X required a one-hour shutdown which temporarily disrupted both the VFD and PCP.

When the motor stops, the relationship between measured torque and fluid submergence breaks down which causes the system to become unobservable due to the degeneracy of the observability matrix. During this shutdown period when the VFD is offline, there is a loss of motor torque and other VFD telemetry. However, the CHP and THP parameters remain continuously available. Since these pressure transmitters are hardwired directly to the IIoT endpoint. They continue to stream live data, as illustrated in Figure 4 .14 where pressure values are actively displayed while VFD parameters indicate "N/A".

Despite the availability of these wellhead pressure readings, the absence of active torque data implies that if the EKF is executed during this period, the Kalman Gain will attempt to correct states based on sensor noise which would lead to large errors and state divergence. The results from the

experiment validate the effectiveness of the supervisory pump state interlock logic. Once an "off" status is detected from the VFD running relay, the logic pauses the EKF measurement update equations and freezes the state estimate.

When the pump is restarted, the surface torque and intake pressure rapidly increase as the annulus refills thus restoring observability to the system. This process introduces transient disturbances due to overcoming static friction and changes in fluid pressure. The reduced-order hydrostatic model assumes steady flow conditions. Therefore, during transient events such as startup, the system experiences highly non-linear multiphase dynamics that the simplified model does not capture. This results in temporary discrepancies between the predicted torque and the actual measured torque.

It was observed that when these torque differences (residuals) exceeded the set confidence limits of ±203.4 Nm (±150 ft-lbs), the observer logic successfully logged the violations using an internal spike counter. After three successive logs on the spike counter, the Submergence status on the dashboard changed from "Normal" to "Anomaly". This change in status highlights periods of low statistical confidence to alert the operator of potential instability in the system.

After the initial startup transients subsided, the hydraulic flow stabilized and the residuals returned to within the acceptable ±203.4 Nm

(±150 ft-lbs) confidence limits. The EKF smoothly converged to the new steady-state submergence level and the supervisory system cleared the Anomaly status and reverted to Normal operation.

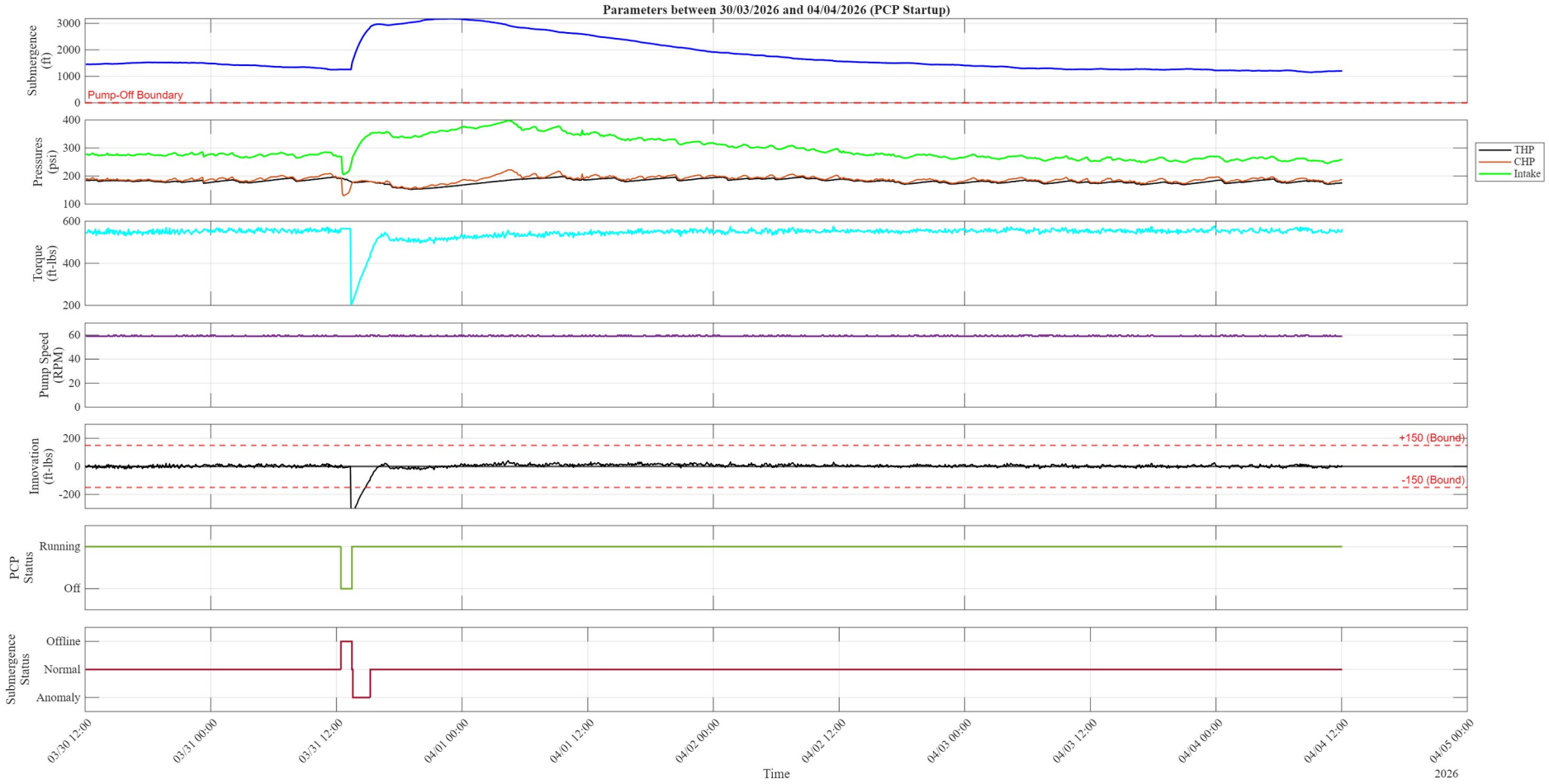

Figure 4.13: Plot of shutdown and restart parameters between 30 March 2026 and 4 April 2026

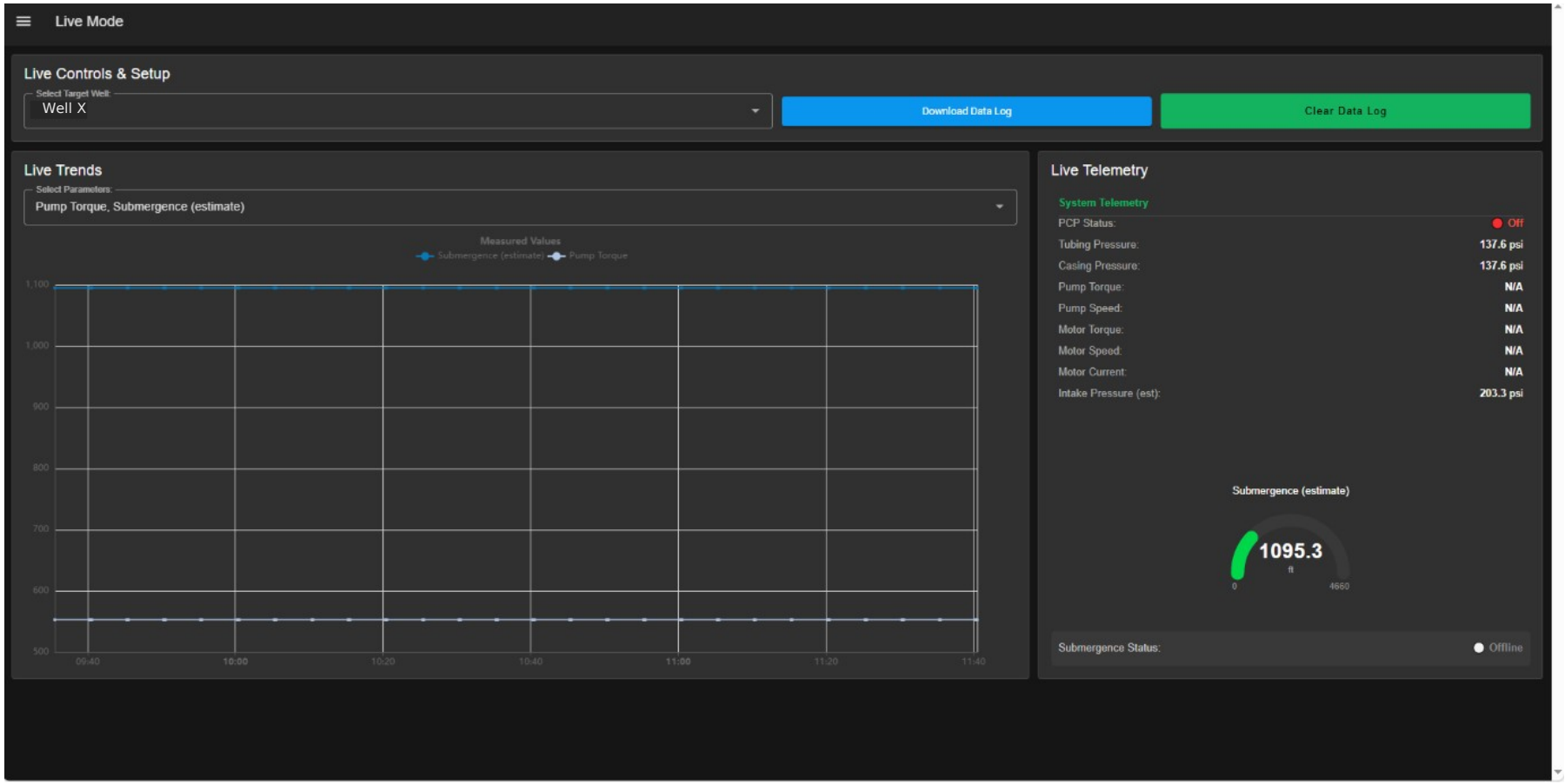

Figure 4.14: Dashboard screenshot illustrating PCP Off status

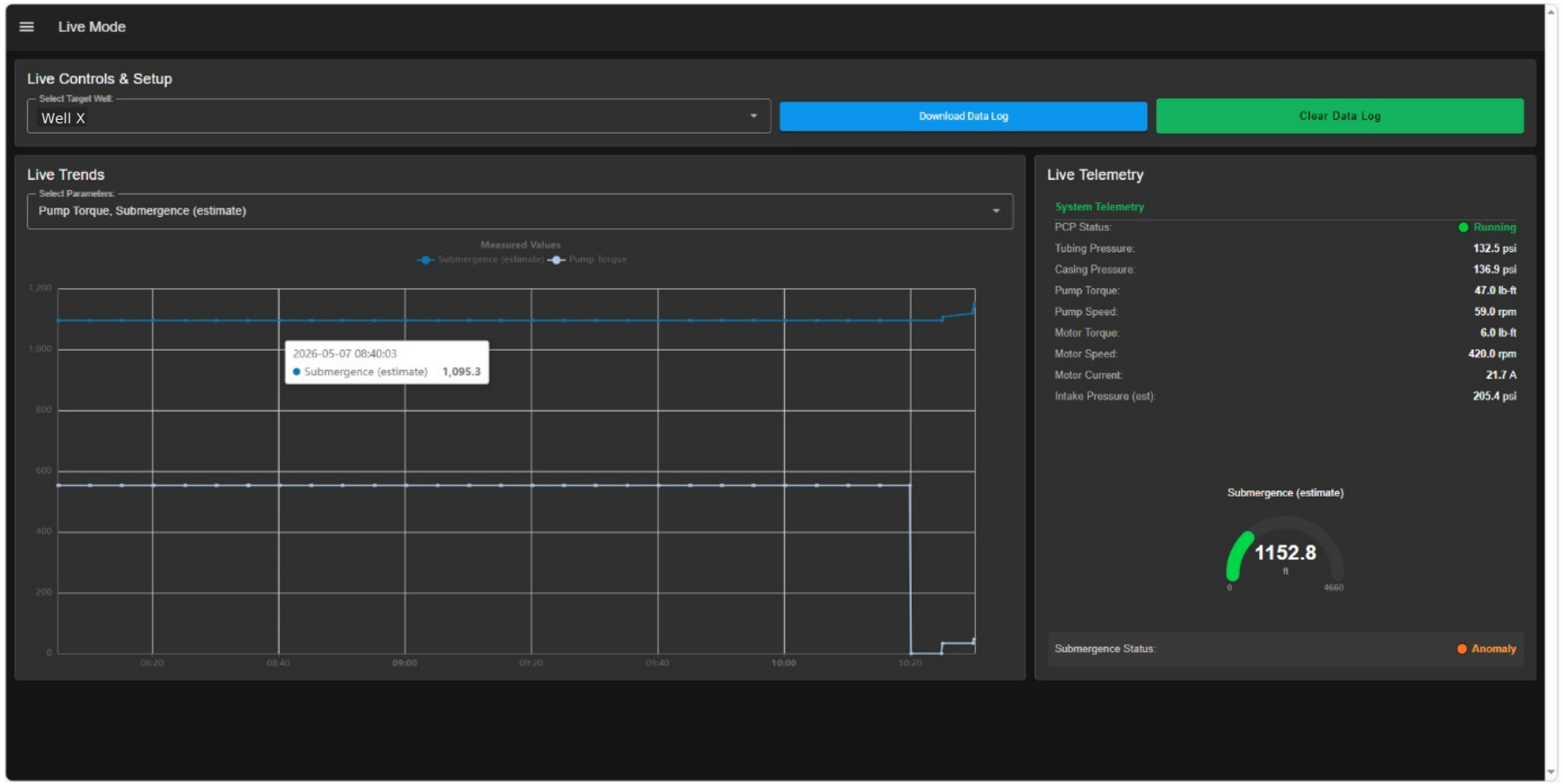

Figure 4.15: Dashboard screenshot illustrating an Anomaly condition

4.6 Open loop Validation of Speed Control

Another project objective was to enable remote supervisory control by modulating the PCP speed setpoint and observe the resulting transient and steady state response. Full closed loop testing was deferred as discussed in Sections 3.6.3 and 3.6.4. Alternatively, the speed modulation sequence was evaluated in an open loop configuration to validate the system's control logic and payload formatting.

In future live deployments, authorized operators will initiate remote speed modulation by entering a new target speed into a restricted, password-protected interface on the company's AVEVA SCADA HMI. While the graphical front end for this control interface was successfully developed as shown in Figure 4 .16, the MQTT integration was not configured for use during the project evaluation period due to resource constraints, as previously discussed in Section 3.6.3. For this validation, a motor speed setpoint of 415 RPM was directly into the Node-RED program as shown in Figure 4 .18.

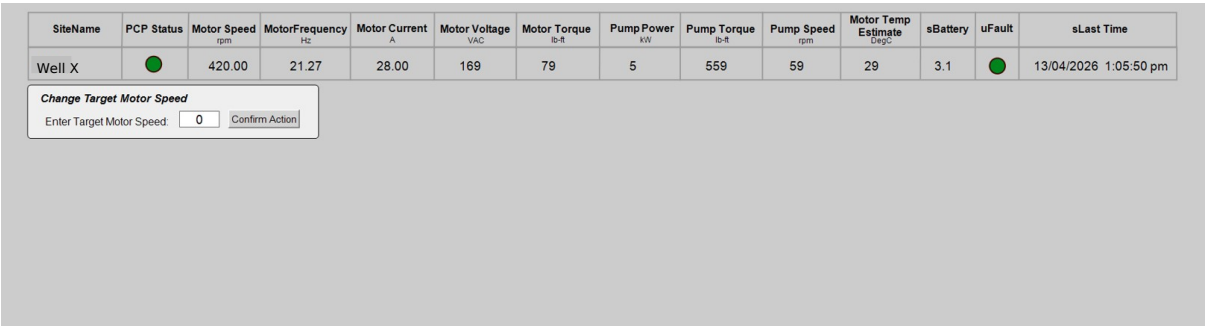

Figure 4.16: AVEVA HMI Screen for Well X

The VoBo HL requires a structured JSON payload that directly corresponds to its Modbus write registers. As demonstrated in the debug output in Figure 4 .18, when the 415 RPM setpoint was injected, the Node-RED logic successfully converted this input to the required JSON payload required for the VoBo HL. This output was cross-referenced with the VolleyBoast Payload Configurator in Figure 4 .17. An accurate Base64 command string match in payload formatting required to execute a Modbus write command on the VoBo endpoint was confirmed.

The command sequence was intentionally halted upstream of the ChirpStack MQTT downlink transmission to complete this open loop test in adherence to the strict operational constraints. This result successfully verifies that the IIoT architecture possesses the required computational logic, payload encoding formatting and bi-directional communication framework required for PCP speed modulation in future deployments.

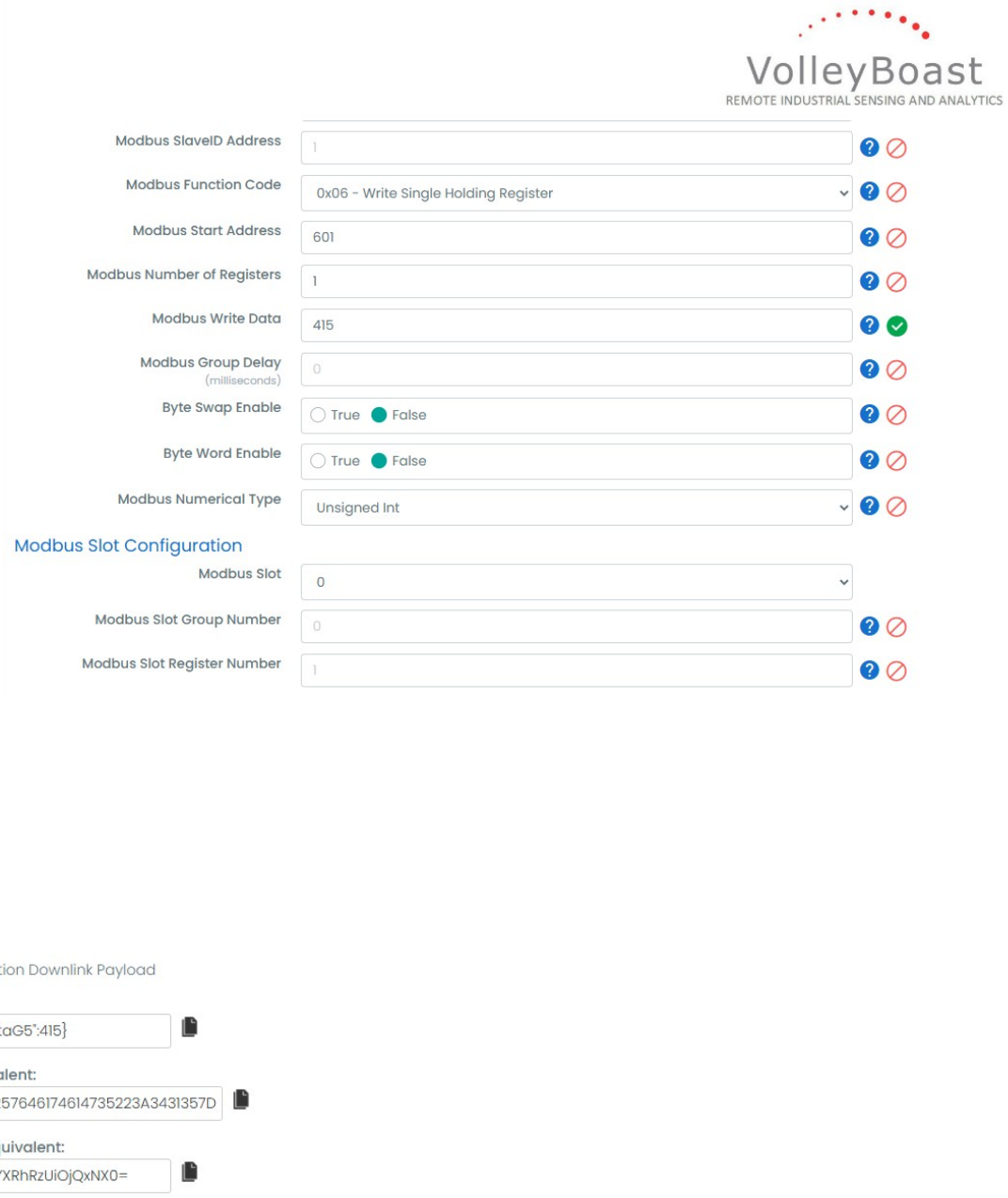

Figure 4.17: VolleyBoast VoBo HL-1 Configuration Downlink Payload screenshot

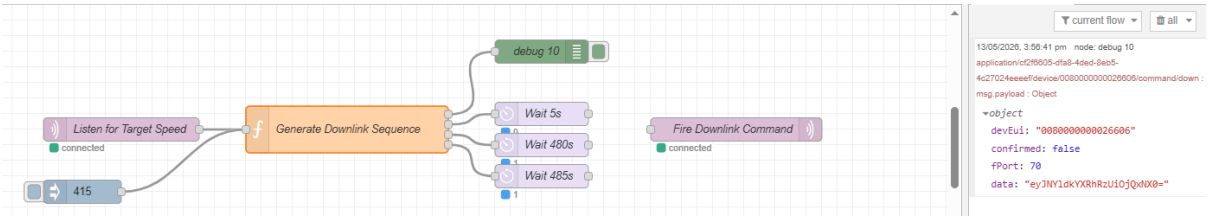

Figure 4.18: Node-RED Speed control nodes and Debug panel

Table 4.4: Summary of Results

Evaluation Scenario	Objectives	Results
Steady-State Estimation	Assess the stability, noise-rejection and estimation accuracy of the EKF virtual sensor.	The EKF consistently tracked downhole fluid submergence without divergence. Achieved a Root Mean Square Error (RMSE) of 54.3 m (178.2 ft) against acoustic shots, representing an error margin of 3.82%.
Simulated Pump-Off Condition	Validate the deterministic friction torque interlock using injected historical telemetry.	Supervisory logic successfully recognized the torque boundary ($T_{meas} \leq \tau_0$), preempted the EKF update, clamped submergence to 0 ft and triggered a "Pump-Off" status to prevent state divergence.
Transient Response (Shutdown & Restart)	Evaluate EKF re-convergence and stability during zero-speed unobservability and start-up transients.	The pump-state interlock successfully paused the EKF during shutdown. Upon restart, the spike counter detected expected torque transients (>150 ft-lbs), triggered an "Anomaly" status and smoothly re-converged to "Normal."
Open loop Validation of Speed Control	Verify the bi-directional control pathway, payload translation and network routing logic.	Node-RED successfully captured a 415 RPM target and accurately formatted the Base64 Modbus payload required for the VoBo endpoint, perfectly matching the vendor configuration tool.

4.7 Engineering and Financial Assessment

4.7.1 Advantages over Prior Control Research

Based on previous research, the most prominent automated optimization architectures have successfully increased production and reduced equipment failures but depends on flow measurement to infer well capacity. The Liquid Inflow Control Method (ICM) and related flow-based strategies such as those developed by (Woolsey 2012), (Romero et al. 2013), (Mehegan and Woolsey 2016) and (Iguaran et al. 2021) modulate pump speed based on the assumption of a linear correlation between RPM and liquid production.

The laboratory analysis of the fluid produced at Well X reported a high viscosity of up to 84,100 cP at 30.0°C (86°F). Under these conditions, wedge flowmeters experience increased pressure losses, distortion of the velocity profile and fouling. Consequently, they are considered technically inaccurate and unreliable for continuous control. This proposed EKF virtual sensor eliminates the hardware dependency by estimating downhole submergence exclusively from surface electrical and mechanical parameters.

Previous studies also explored Kalman filtering for PCP optimization. (Ceballos and Vivas 2019) proposed utilizing a Kalman observer within a Linear Quadratic Regulator (LQR) to maximize oil production. However, their methodology relied on downhole intake pressure sensors and the

implementation was conducted entirely within a numerical simulation environment. Furthermore, their estimated submergence state was not independently verified against physical measurements, as a result the physical accuracy of the observer was unquantified under real operating conditions.

The methodology presented in this research bridges this critical gap between simulation and field deployment. The EKF was deployed as a standalone virtual sensor within a live, continuous IIoT architecture and operated without any downhole instrumentation. Furthermore, the virtual sensor was directly validated against independent acoustic fluid-shot measurements. The achieved Root Mean Square Error (RMSE) of 54.3 m (178.16 ft) and an error margin of less than 4% across the 1,420.4 m (4,660 ft) well depth proves that observer-based submergence estimation is accurate and scalable for real world PCP supervisory control.

4.7.2 Economics and Risk Mitigation

The financial assessment of the IIoT virtual sensor architecture evaluates both the initial Capital Expenditure (CAPEX) required for deployment and the operational values realized over a one year operational cycle. All financial metrics are presented with their respective conversions assuming a standard exchange rate of TT$ 6.78 = USD $1.00.

Table 4 .5 provides a comparative breakdown of the CAPEX required per well for the existing proprietary solution vs this proposed IIoT

architecture. The costs for the PCP and VFD remain constant across both solutions and are therefore excluded. The proprietary solution requires specialized, proprietary hardware along with mandatory vendor commissioning and startup fees. Conversely, this IIoT architecture leverages commercially available components, requiring only the VolleyBoast VoBo HL-1 endpoint, two pressure transmitters for the CHP and THP measurements and the required cables for interconnection. The network integration is executed entirely by Company X in-house personnel therefore setup costs are reduced to zero.

Table 4.5: CAPEX Per Well Breakdown

Component	**Proprietary Third-Party Solution**	**Proposed IIoT Architecture**
Controller	TT$ 71,088.85 *(Foresite Edge Controller)*	TT$ 7,000.00 *(VolleyBoast VoBo HL-1)*
Sensors	TT$ 34,645.16 *(Foresite Edge Probes)*	TT$ 9,000.00 *(2x Murphy Pressure Transmitters @ TT$4,500 ea.)*
Cabling	TT$ 7,298.37 *(Foresite Edge Cable Assembly)*	TT$ 0.00 *(Utilizes company stock cables)*
Commissioning & Startup	TT$ 3,481.35 *(Foresite One-Time Setup Fee)*	TT$ 0.00 *(In-house deployment)*
Total CAPEX	TT$ 116,513.73 (USD $17,185.00)	TT$ 16,000.00 (USD $2,360.00)

Over a one year operational cycle, the architecture provides measurable improvements in the following areas:

- **OPEX Elimination:** Proprietary monitoring solutions impose recurring operational expenditures to maintain cloud connectivity. Company X currently incurs an annual cost of approximately TT$ 378,830 (USD $55,872) to maintain third-party monitoring on 24 PCP wells (TT$ 15,784 (USD $2,328) per well annually). Routing telemetry through the self-hosted Node-RED server and ChirpStack LoRaWAN network eliminates these recurring subscription fees. However, the VoBo HL endpoint introduces a recurring consumable OPEX of TT$ 384 (USD $57.00) per well annually for battery replacement. Accounting for this consumable, this system yields a net one year fleet wide OPEX savings of TT$ 369,600 (USD $54,513).

- **Productivity and Revenue Enhancement:** Continuous estimation of submergence allows the PCP speed to be optimized to match reservoir inflow. Previous industry optimization methods recorded production increases between 7% and 20%. For Well X, a baseline of 252 barrels of oil per day (BOPD) at an average of USD $70/bbl (TT$ 474.60/bbl) was adopted for the economic evaluation (EIA 2026). This price represents a conservative planning assumption consistent with recent Brent crude oil forecasts and prevailing market conditions. For a conservative 5% production improvement scenario, the additional

production of 12.6 BOPD would generate approximately USD $321,930 (TT$ 2,182,685) in incremental annual revenue per well, scaling to a potential USD $7,726,320 (TT$ 52,384,450) across the 24-well fleet annually.

- **Downtime Reduction and Cost Avoidance:** The repair of a catastrophic stator failure caused by a pump-off condition requires a rig-assisted workover intervention which incurs costs of approximately USD $3,000,000 (TT$ 20,340,000) per event. The deterministic friction torque interlock protects the PCP from this failure mode. The prevention of these failures also avoids the deferred production associated with the well being shut-in while awaiting rig availability.

- **Supervision and Manpower Optimization:** Company X currently relies on routine monthly manual acoustic fluid-level shots to verify wellbore hydrodynamics which requires dispatching a minimum two-man technician crew for approximately 4 hours (8 labour hours) per well. The EKF virtual sensor provides continuous remote visibility via the SCADA HMI screen, shifting this requirement from a monthly diagnostic routine to a potentially semi-annual recalibration schedule. By reducing the frequency of acoustic shots from twelve to two per year, the system recovers 80 labor-hours per well annually. At a

standard technician rate of TT$ 156.24/hr, this results in a fleet-wide labor cost savings of TT$ 299,980.80 (USD $44,245) per year.

4.7.3 Investment Feasibility

A financial analysis was conducted to map the previously defined operational values into a formal one year revenue evaluation. The feasibility study models two distinct deployment realities, a Greenfield scenario for new asset expansions (Scenario A) and a Brownfield scenario for retrofitting existing assets (Scenario B).

An $N+m$ sparing strategy was incorporated to guarantee reliable operations while avoiding the unnecessary accumulation of capital in unused inventory within the deployment modes. In this framework, "N" represents the active wells and "m" represents a finite contingency stock based on a strict ratio of one complete spare well set for every five active wells.

The USD $3,000,000 (TT$ 20,340,000) cost associated with catastrophic stator failures was classified as a contingency expense and excluded from the analysis since it represents risk mitigation rather than direct revenue generation.

4.7.3.1 Scenario A: Greenfield Deployment (The 25th Well)

This scenario evaluates the financial implications of expanding the asset base by adding a new well. If the Company selects the traditional

proprietary architecture, it incurs a hardware CAPEX of TT$ 116,513.73 (USD $17,185.00). Conversely, selecting this proposed IIoT solution requires a significantly lower hardware CAPEX of TT$ 16,000.00 (USD $2,360.00).

A contingency stock of m=1 complete replacement set (one VoBo endpoint and two pressure transmitters) is necessary to maintain an adequate inventory management strategy based on a 1-to-5 N+m sparing ratio to a single-well asset (N=1). This requirement adds a dedicated spare parts CAPEX of TT$ 16,000.00 (USD $2,360.00) to the IIoT framework resulting in a total initial investment to TT$ 32,000.00 (USD $4,720.00).

During the Year 1 operational cycle, the proprietary route incurs an ongoing expense of TT$ 15,784.00 (USD $2,328.00) for telemetry subscriptions and TT$ 14,999.04 (USD $2,212.25) for manual acoustic shot labor. In contrast, the IIoT architecture eliminates telemetry fees and reduces acoustic labor to TT$ 2,499.84 (USD $368.71). Additionally, it includes a battery maintenance fee of TT$ 384.00 (USD $57.00) and results in TT$ 2,182,685.00 (USD $321,930.00) in optimized oil revenue.

When the respective CAPEX from these operational revenues is subtracted, this results in a Net one year Revenue of -USD $21,725.25 (-TT$ 147,296.77) for the proprietary option compared to a highly profitable +USD $316,784.29 (+TT$ 2,147,794.20) for the IIoT design.

4.7.3.2 Scenario B: Brownfield Retrofit (The 24-Well Fleet)

This scenario evaluates the financial rationale for replacing the existing proprietary equipment across the active 24-well fleet and replacing it with this IIoT architecture. In this evaluation, it should be noted that no CAPEX savings can be claimed for the for the purchase price of the existing proprietary hardware.

The implementation of IIoT infrastructure across all 24 wells requires an upfront CAPEX of TT$ 384,000.00 (USD $56,637.00). Utilizing the 1-to-5 $N+m$ sparing ratio to the 24 active wells ($N=24$) requires maintaining a contingency stock of $m=5$ complete spare sets. The associated costs for these five VoBo endpoints and ten pressure transmitters introduce a fleet spare CAPEX of TT$ 80,000.00 (USD $11,799.41), resulting in a total initial investment of USD $68,436.41 (TT$ 464,000.00).

On an annual basis, the maintenance of the proprietary fleet incurs an ongoing expenditure of TT$ 378,816.00 (USD $55,872.00) for recurring cloud subscriptions and TT$ 359,976.96 (USD $53,094.00) for acoustic shots labor. In contrast, this IIoT architecture eliminates telemetry costs, reduces overall labor expenses to TT$ 59,996.16 (USD $8,849.00), incurs TT$ 9,216.00 (USD $1,359.00) in battery costs and generates optimized production revenue totaling USD $7,726,320.00 (TT$ 52,384,450.00).

After deducting the retrofit and spare parts CAPEX, the IIoT architecture yields a significant Net one year Revenue of USD

$7,688,205.18 (TT$ 52,126,030.80), effectively reversing the continuous financial impact by the legacy proprietary configuration.

The one year economic impact and financial revenue comparison across all options is summarized in Table 4 .6.

Table 4.6: Consolidated One Year Financial Summary

Financial Metric & Operational Value	**Evaluation Metric**	**Scenario A: Greenfield (1 Well)**	**Scenario A: Greenfield (1 Well)**	**Scenario B: Brownfield (24 Wells)**	**Scenario B: Brownfield (24 Wells)**
		Proprietary	**Proposed IIoT**	**Proprietary Baseline**	**IIoT Retrofit**
CAPEX (Year 0)	Hardware & Installation	USD 17,185.00 (TT 116,513.73)	USD 2,360.00 (TT 16,000.00)	USD 0.00 (TT 0.00)	USD 56,637.00 (TT 384,000.00)
N+m Spares CAPEX (Year 0)	Contingency Stock	USD 0.00 (TT 0.00)	USD 2,360.00 (TT 16,000.00)	USD 0.00 (TT 0.00)	USD 11,799.41 (TT 80,000.00)
Operating Revenue (Year 1)					
o Telemetry Subscription OPEX	Proprietary Cloud vs Self-Hosted	−USD 2,328.00 (−TT 15,784.00)	USD 0.00 (TT 0.00)	−USD 55,872.00 (−TT 378,816.00)	USD 0.00 (TT 0.00)
o Consumable OPEX (Battery)	Annual Power Replacement	USD 0.00 (TT 0.00)	-USD 57.00 (−TT 384.00)	USD 0.00 (TT 0.00)	−USD 1,359.00 (−TT 9,216.00)
o Supervision & Labor OPEX	Acoustic Shots *(2-Man Crew @ TT$ 156.24/hr)*	−USD 2,212.25 (−TT 14,999.04)	−USD 368.71 (−TT 2,499.84)	−USD 53,094.00 (−TT 359,976.96)	−USD 8,849.00 (−TT 59,996.16)
o Production Optimization Revenue	Optimized Drawdown (+5% on 252	USD 0.00 (TT 0.00)	+USD 321,930.00 (+TT	USD 0.00 (TT 0.00)	+USD 7,726,320.00 (+TT

Financial Metric & Operational Value	**Evaluation Metric**	**Scenario A: Greenfield (1 Well)**	**Scenario A: Greenfield (1 Well)**	**Scenario B: Brownfield (24 Wells)**	**Scenario B: Brownfield (24 Wells)**
		Proprietary	**Proposed IIoT**	**Proprietary Baseline**	**IIoT Retrofit**
	BOPD)		2,182,685.00)		52,384,450.00)
Total Year 1 Operating Revenue		−USD 4,540.25 (−TT 30,783.04)	USD 321,504.29 (TT 2,179,801.16)	−USD 108,966.00 (−TT 738,792.96)	USD 7,716,112.00 (TT 52,315,237.84)
Net one year Revenue		−USD 21,725.25 (−TT 147,296.77)	USD 316,784.29 (TT 2,147,794.20)	−USD 108,966.00 (−TT 738,792.96)	USD 7,647,675.59 (TT 51,851,237.84)
Contingency Risk Mitigated	Catastrophic Stator Failure Mitigation	High Risk / Lagging	USD 3,000,000.00 (TT 20,340,000.00)	High Risk / Lagging	USD 3,000,000.00 (TT 20,340,000.00) *Per Well*

The financial analysis of these two scenarios clearly demonstrates the economic viability of the proposed IIoT architecture therefore, it is advisable to pursue this implementation. Additionally, consideration should be given to its broader adoption across the fleet, including any necessary adjustments, provided that subsequent deployments remain financially feasible.

4.8 Limitations and Future Work

While the proposed EKF virtual sensor and IIoT supervisory framework successfully achieved its design objectives, the system is bounded by specific mathematical and operational constraints.

4.8.1 Limitations

The current implementation of the virtual sensing and control architecture is subject to the following practical limitations:

- **IIoT Endpoint Update Rate:** The IIoT endpoint currently wakes up at a nominal five-minute interval, which restricts the EKF's frequency response, parameter updates and speed modulation actuation. To mitigate this, a one-minute update interval was successfully field tested and is scheduled for permanent integration upon the final commissioning of the closed loop speed control. While this accelerated sampling frequency effectively improves the under sampling and latency constraints, it introduces a trade-off by reducing the battery life of the IIoT endpoint.
- **Static Parameter Bias:** Mechanical Friction (τ_0) and Tubing Gradient $(Grad_{Liq})$ are configured as static variables, long-term physical shifts in the wellbore (e.g., a gradual increase in water cut or PCP wear) will introduce a systematic bias into the submergence estimate. Currently, mitigating this drift requires manual recalibration of the variables in Node-RED.

- **SACADA Alarm Integration:** The virtual sensor's submergence estimates and system status alerts (e.g., Normal, Anomaly, Pump-Off) are visualized exclusively on the standalone Node-RED dashboard. As a result, control room operators would be required to monitor a secondary screen to evaluate PCP parameters.
- **Open loop Actuation:** Due to stringent operational constraints and mechanical risks to the PCP, the actuation pathway was limited to an open loop digital validation as described in Section 3.6.4.

4.8.2 Recommendations for Future Work

The following enhancements are recommended for future research to address the current limitations:

1. **Adaptive Covariance:** Multiphase flow often generates fluid slugs which violate the EKF's statistical assumptions. Therefore, future work should transition to an Adaptive Extended Kalman Filter. The detection of statistical outliers in real-time could inflate the measurement noise covariance (R) and suppress the Kalman Gain during transients allowing the estimator to reject noisy data.
2. **Closed loop Control Implementation:** In addition to the recommendations in section 3.6.4 Closed Loop Speed Control Live Commissioning (Future), future work should introduce Proportional-Integral (PI) control logic to close the control loop. This will allow the fluid level to be maintained at a target setpoint without human

intervention. The system would be able to automatically generate and send LoRaWAN downlinks to change the VFD speed, using the estimated submergence from the EKF as the feedback variable.

3. **SCADA Alarm Integration:** Currently, the virtual sensor's dynamic submergence estimates and system statuses (e.g., Normal, Anomaly, Pump-Off) are visualized only on the Node-RED dashboard. To centralize operational awareness, focus should be directed on integrating these alerts directly into the company’s AVEVA SCADA alarm management system.

   This can be achieved by configuring Node-RED to publish system statuses as integer-based MQTT payloads (e.g., 0 = Normal, 1 = Anomaly, 2 = Pump-Off) back to the Cogent DataHub. The AVEVA System Application Server can then subscribe to these specific MQTT topics. Once in the AVEVA environment, the integer tags can be mapped to specific graphical alarms. This integration would ensure that control room operators receive predictive pump-off warnings directly on their main SCADA screens.

5 Conclusion

The objective of this project was to design, implement and validate an EKF based submergence sensor and supervisor control architecture for speed-controlled PCP systems. A reduced-order state-space model was developed to correlate surface-measured electrical and mechanical parameters with the downhole hydrostatic fluid load. This model was then used to create a real-time virtual sensor using an EKF. Previous research relied on downhole sensors, unreliable surface flowmeters or purely mathematical simulations however this project establishes a new baseline. It successfully demonstrates the first field deployment and validation of a sensorless, surface-driven EKF on an active, heavy-oil production asset.

The performance of the EKF submergence estimator was evaluated on Well X and compared against acoustic fluid-shot measurements. This resulted a Root Mean Square Error (RMSE) of 54.3 m (178.2 ft) and an error margin of 3.82% across the 1,420.4 m (4,660-ft) wellbore. Due to the novelty of this research, the 3.82% error margin establishes a new baseline for the accuracy of sensorless submergence estimation on a live asset. Furthermore, the system's supervisory control capabilities were successfully verified through an open loop validation pathway. In this validation, the Node-RED architecture accurately captured target setpoints from the AVEVA SCADA back-end, scaled the inputs and compiled the

Base64-encoded Modbus commands required for bi-directional IIoT communication.

The significance of this technical accuracy translates into substantial, scalable commercial value. When applied to the Company’s 24-well fleet over a one year operational cycle, this solution is projected to generate a net one year revenue of USD $7,647,675.59 (TT$ 51,851,237.84). The implementation of the virtual sensor facilitates optimized pressure drawdown which has the potential to enhance production throughput by 5%, resulting in an estimated additional operating revenue of USD $7,726,320.00 (TT$ 52,384,450.00). Furthermore, the precision of the state estimation enables the deterministic pump-off interlock to actively safeguard against dry-run stator failures. Avoiding a catastrophic failure translates to a risk cost avoidance of USD $3,000,000.00 (TT$ 20,340,000.00) per well.

Additionally, the adoption of the self-hosted IIoT architecture leads to a consolidated one year expense reduction of TT$ 669,580.80 (USD $98,758.00) by minimizing capital expenditures on proprietary hardware, eliminating recurring telemetry operating expenses and shifting routine manual acoustic fluid shots to a semi-annual recalibration schedule. Based on these financial assessments, pursuing implementation and considering broader adoption across the field is highly recommended.

While the system achieved its design objectives, it operates under specific constraints. The mathematical model relies on static parameters,

such as a constant fluid gradient and fixed mechanical friction which can vary with reservoir conditions, potentially leading to estimation errors over time if not recalibrated. Additionally, the transient response is limited by the five-minute LoRaWAN telemetry update rate. Finally, due to the severe mechanical risks associated with inducing mechanical stress on an active rod string, live closed loop speed modulation was limited to open loop validation during this phase, deferring live actuation pending further risk assessments and complete SCADA HMI integration.

6 References

ABB. 2011. Direct torque control: The world's most advanced AC drive technology. Technical Guide No. 1. Helsinki: ABB Oy.

Ahmad, S., and H. Le. 2023. Effectiveness of field oriented control and direct torque control methods for induction motor speed regulation. Doctoral dissertation, California State Polytechnic University, Pomona.

Al-Safran, E., A. Aql, and T. Nguyen. 2017. Analysis and prediction of fluid flow behavior in progressing cavity pumps. *Journal of Fluids Engineering* 139 (12): 121102.

Ceballos, J. B., and Ó. A. Vivas. 2019. Mathematical model of controllers for progressive cavity pumps. *Revista UIS Ingenierías* 18 (2): 17-29.

Eggers, J., A. E. Gomez, Y. Hurtado, A. Claib, T. Silva, G. J. Nunez, J. Borjas, L. Duarte, and S. Valbuena. 2013. Achieving production optimization using progressive cavity pumps, artificial neural networks and system-based monitoring. In *SPE Canada Heavy Oil Conference* proceedings, SPE-165482. Richardson, TX: Society of Petroleum Engineers.

EIA. 2026. Short-term energy outlook. https://www.eia.gov/outlooks/steo/ (accessed July 11, 2026).

Fotsa, R. T., B. P. Ndemanou, A. S. K. Tsafack, N. F. F. Foka, and D. S. Fouazong. 2024. Production of a dead oil well by a progressive cavity pump and its optimization. *Iraqi Journal of Chemical and Petroleum Engineering* 25 (3): 15-20.

Gamboa, J., O. Aurelio, and E. Sorelys. 2003. New approach for modeling progressive cavity pumps performance. In *SPE Annual Technical Conference and Exhibition* proceedings, SPE-84137. Richardson, TX: Society of Petroleum Engineers.

Gelb, A., ed. 1974. *Applied optimal estimation*. Cambridge, MA: MIT Press.

González, D., A. Badias, I. Alfaro, F. Chinesta, and E. Cueto. 2017. Model order reduction for real-time data assimilation through extended Kalman filters. *Computer Methods in Applied Mechanics and Engineering* 326: 679-693.

Jazwinski, A. H. 1970. *Stochastic processes and filtering theory*. New York: Academic Press.

Kani, J. N., and A. H. Elsheikh. 2019. Reduced-order modeling of subsurface multi-phase flow models using deep residual recurrent neural networks. *Transport in Porous Media* 126 (3): 713-741.

Klein, S. T., W. B. Thrasher, L. Mena, E. Quijada, and C. Brunings. 1999. Well optimization package for progressive cavity pumping systems. In *SPE*

Oklahoma City Oil and Gas Symposium / Production and Operations Symposium proceedings, SPE-52162. Richardson, TX: Society of Petroleum Engineers.

Kouhi, H., M. Kabganian, and M. Shahravi. 2020. Extended Kalman filter–based state and parameter estimation for nonlinear mechanical systems with friction. *ISA Transactions* 99: 528–540.

Lea, J. F., H. V. Nickens, and M. R. Wells. 1999. Gas well liquid loading and deliquification. *SPE Production & Facilities* 14 (2): 89–95.

Lehman, M. 2004. Progressing cavity pumps in oil and gas production. *World Pumps* 2004 (457): 20-22.

Mehegan, L., and K. A. Woolsey. 2016. Using liquid inflow method to optimize progressive cavity pumps. In *SPE Artificial Lift Conference and Exhibition-Americas* proceedings, D031S009R001. Richardson, TX: Society of Petroleum Engineers.

Nguyen, K., T. C. Nguyen, and E. Al-Safran. 2021. Modeling the performance of progressive cavity pump under downhole conditions. *Journal of Petroleum Science and Engineering* 198: 108121.

Nguyen, T., E. Al-Safran, A. Saasen, and O. M. Nes. 2014. Modeling the design and performance of progressing cavity pump using 3-D vector approach. *Journal of Petroleum Science and Engineering* 122: 180-186.

Nguyen, T., H. Tu, E. Al-Safran, and A. Saasen. 2016. Simulation of single-phase liquid flow in progressing cavity pump. *Journal of Petroleum Science and Engineering* 147: 617-623.

Palm, W. J., III. 2013. *System dynamics*. 3rd ed. New York: McGraw-Hill.

Pessoa, P. A. S., E. E. Paladino, and J. A. Lima. 2009. A simplified model for the flow in a progressive cavity pump. In *The 20th International Congress of Mechanical Engineering* proceedings.

Qin, S. J., and T. A. Badgwell. 2003. A survey of industrial model predictive control technology. *Control Engineering Practice* 11 (7): 733–764.

Romero, A., A. Gasparri, and E. Ferrigno. 2013. PCP production optimization in real time with surface controller. In *SPE Artificial Lift Conference-Latin America and Caribbean* proceedings, SPE-165057. Richardson, TX: Society of Petroleum Engineers.

Saveth, K. J., and S. T. Klein. 1989. The progressing cavity pump: Principle and capabilities. In *SPE Oklahoma City Oil and Gas Symposium / Production and Operations Symposium* proceedings, SPE-18873. Richardson, TX: Society of Petroleum Engineers.

Simon, D. 2006. *Optimal state estimation: Kalman, H∞, and nonlinear approaches*. Hoboken, NJ: John Wiley & Sons.

Stout. 2025. The limits of PV-10 in oil & gas reserve valuation. https://www.stout.com/en/insights/article/limits-pv10-oil-gas-reserve-valuation (accessed July 11, 2026).

Takács, G. 2010. *Electrical submersible pumps manual: Design, operations, and maintenance*. Oxford: Gulf Professional Publishing.

Tiitinen, P., and M. Surandra. 1996. The next generation motor control method, DTC direct torque control. In *Proceedings of International Conference on Power Electronics, Drives and Energy Systems for Industrial Growth*, 37-43. IEEE.

Wagg, B. T. 2002. Development of a standard for progressing cavity pumping systems surface drives. In *PETSOC Canadian International Petroleum Conference* proceedings, PETSOC-2002. PETSOC.

Welch, G., and G. Bishop. 2006. An introduction to the Kalman filter. University of North Carolina at Chapel Hill, Department of Computer Science.

White, F. M. 2015. *Fluid mechanics*. 8th ed. New York: McGraw-Hill Education.

Woolsey, K. A. 2012. Improving progressing-cavity-pump performance through automation and surveillance. *Journal of Canadian Petroleum Technology* 51 (1): 74-81.

Zheng, L., X. Wu, G. Han, H. Li, Y. Zuo, and D. Zhou. 2018. Analytical model for the flow in progressing cavity pump with the metallic stator and rotor in clearance fit. *Mathematical Problems in Engineering* 2018 (1): 3696930.

Zhou, D., and H. Yuan. 2008. Design of progressive cavity pump wells. In *SPE Progressing Cavity Pumps Conference* proceedings, SPE-113324. Richardson, TX: Society of Petroleum Engineers.

Appendix A